Journal of Medicinal Chemistry

Article

Structure-based design of potent and selective inhibitors of the metabolic kinase PFKFB3

Scott Boyd, Joanna Brookfield, Susan E. Critchlow, Iain Cumming, Nicola Curtis, Judit Debreczeni, Sébastien Louis Degorce, Craig Donald, Nicola J Evans, Sam Groombridge, Philip Hopcroft, Neil Jones, Jason Grant Kettle, Scott Lamont, Hilary Lewis, Philip A MacFaul, Sheila Mcloughlin, Laurent Rigoreau, James Smith, Steve St-Gallay, Julie Stock, Andrew Turnbull, Edward Wheatley, Jon Winter, and Jonathan Wingfield

J. Med. Chem., **Just Accepted Manuscript** • DOI: 10.1021/acs.jmedchem.5b00352 • Publication Date (Web): 07 Apr 2015

Structure-based design of potent and selective inhibitors of the metabolic kinase PFKFB3

Scott Boyd,[†] Joanna L. Brookfield,[‡] Susan E. Critchlow,[†] Iain A. Cumming,[‡] Nicola J. Curtis,[†] Judit Debreczeni,[†] Sébastien L. Degorce,[†] Craig Donald,[†] Nicola J. Evans,[§] Sam Groombridge,[†] Philip Hopcroft,[†] Neil P. Jones,[§] Jason G. Kettle,[†*] Scott Lamont,[†] Hilary J. Lewis,[†] Philip MacFaull,[†] Sheila B. McLoughlin,[‡] Laurent J. M. Rigoreau,[‡] James M. Smith,[‡] Steve St-Gallay,[†] Julie K. Stock,[§] Andrew P. Turnbull,[§] Edward R. Wheatley,[§] Jon Winter,[†] Jonathan Wingfield[†]

[†]Oncology Innovative Medicines Unit, AstraZeneca, Mereside, Alderley Park, Macclesfield, Cheshire SK10 4TG, United Kingdom

[‡]CRT Discovery Laboratories, Jonas Webb Building (B910), Babraham Research Campus, Cambridge, CB22 3AT, United Kingdom

[§]CRT Discovery Laboratories, Wolfson Institute for Biomedical Research, University College London, The Cruciform Building, Gower Street, London, WC1E 6BT, United Kingdom

ABSTRACT

A weak screening hit with suboptimal physicochemical properties was optimized against PFKFB3 kinase using critical structure-guided insights. The resulting compounds demonstrated high selectivity over related PFKFB isoforms and modulation of the target in a cellular context. A selected example demonstrated exposure in animals following oral dosing. Examples from this series may serve as useful probes to understand the emerging biology of this metabolic target.

INTRODUCTION

In the transition to a malignant phenotype and in response to an increased energy demand driven by increased rates of proliferation, cancer cells generate energy by glycolysis in a process marked by increased glucose uptake and lactate production. This switch from the oxidative phosphorylation observed in normal cells was first described by Otto Warburg over half a century ago,[1] and is the basis on which the non-invasive diagnostic imaging technique ^{18}FDG-PET relies.[2] Phosphofructokinase 1 (PFK1) catalyses the conversion of fructose-6-phosphate (F6P) and ATP to fructose-1,6-bisphosphate (F-1,6-BP) and ADP. This irreversible reaction is one of the rate limiting steps of glycolysis, and the activity of this enzyme is regulated by a number of cellular metabolites,[3] including ATP/AMP ratio, citrate, *p*H and the allosteric activator fructose-2,6-bisphosphate (F-2,6-BP),[4] which is the product of phosphofructokinase 2 (PFK2). PFK2 is a bi-functional 6-phosphofructo-2-kinase/fructose-2,6-biphosphatase.[5,6] Both kinase and phosphatase reactions are catalysed within the same polypeptide chain, which contains an N-terminal kinase domain and a C-terminal phosphatase domain. Several isoforms of PFK2 have been identified, and are encoded by 4 genes, PFKFB1-4. Of these, PFKFB3 is

reported to have the highest kinase to phosphatase ratio,[7] approximately 700 times in favour of the production of F-2,6-BP.

PFKFB3 is over-expressed in a wide variety of cancers including breast, prostate, colon, astrocytoma and ovarian cancers, and its expression and/or activity is found to correlate strongly with aggressiveness/poor prognosis in colon, breast, ovarian and thyroid tumors.[8] PFKFB3 protein is highly phosphorylated in human cancer tissue when compared with corresponding normal tissue, suggesting differential regulation in a cancer setting.[9] Further evidence reveals that PFKFB3 is essential for Ras-dependent glycolysis and transformation in lung fibroblast models.[10] High glycolytic flux is essential for tumor growth in hypoxic conditions and a further mode of PFKFB3 regulation is through the hypoxia-inducible factor-1 (HIF-1) pathway. HIF-1 binds to the PFKFB3 promoter and up-regulates expression in response to hypoxia both *in vitro* and *in vivo*.[11,12] High glycolytic activity is also observed in certain normal tissue or organs with high glucose demands (i.e. brain) and there is some evidence that PFKFB3 may have roles in rapidly proliferating normal cells (i.e. astrocytes and T-lymphocytes).[13,14] Therefore as with many metabolism targets it is important to consider the impact of inhibition of PFKFB3 in normal tissues.

There are limited reports on potent and selective inhibitors of PFKFB3 kinase. The most widely studied agent is undoubtedly 3-(3-pyridinyl)-1-(4-pyridinyl)-2-propen-1-one **1** (termed 3PO),[15] and optimization has recently led to a more potent analogue **2** being reported (PFK15).[16] A range of biological activity has been ascribed to this series including reduction in F-2,6-BP

levels, inhibition of glucose uptake and lactate production, and induction of apoptosis in cancer cell lines both *in vitro* and *in vivo*. It is unclear however whether all of these effects are attributable solely to direct effects on PFKFB3 kinase since the potency of the observed cellular phenotypes appear in some cases at odds with its modest kinase inhibitory activity. 3PO itself has been shown to display both competitive and uncompetitive inhibition with respect to isolated PFKFB3 kinase, and whilst it is true that expression of PFKFB3 leading to increased intracellular levels of F-2,6-BP can protect Jurkat cells from the cytotoxic effects of 3PO, additional off-target effects cannot be ruled out. A recent report disclosing pyridazinone inhibitors of PFKFB3 such as **3**,[17] highlights that neither **1** nor **3** showed glycolytic pathway cellular activity that could be separated from cytotoxicity at the concentrations used, and that the reported enzyme inhibitory activity of **2** itself could not be validated (IC_{50} > 1000 μM versus 0.2 μM reported). In our hands, 3PO itself is inactive in a PFKFB3 kinase assay (IC_{50} > 100 μM) and no crystal structure is available confirming binding of 3PO or analogues to PFKFB3 kinase. Herein we report our own efforts to obtain potent and selective inhibitors of PFKFB3 kinase which may serve as useful tools to further understand the biology of this interesting target.

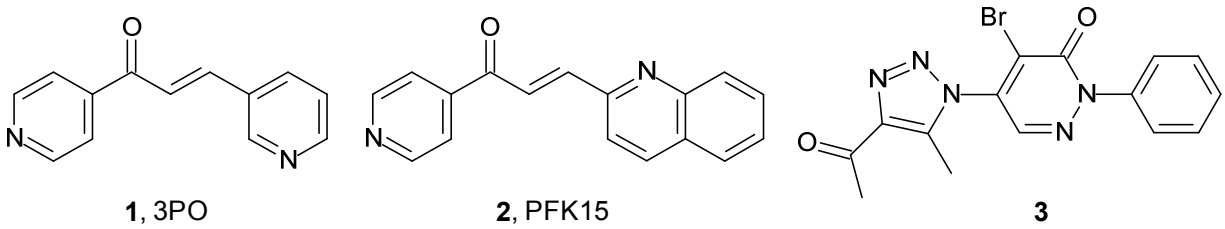

1, 3PO **2**, PFK15 **3**

Figure 1. Chemical structures of known PFKFB3 inhibitors

CHEMISTRY

A number of diverse approaches were taken to synthesize the compounds studied, with routes to representative examples summarized in Schemes 1-5 (full details are available for all compounds in the Supplementary Information). The syntheses of 2-amino-5-phenoxyindoles such as **11** is illustrated in Scheme 1 with the initial step being a S_NAr reaction between 5-chloro-2-nitroaniline **4** and the phenol **5**. This reaction proceeds in good yield using sodium hydride/dimethylacetamide conditions. Standard diazotization conditions give rise to the *o*-chloronitro compound **7** which can then undergo reaction with malononitrile which upon *in situ* sodium dithionite reduction cyclizes to generate the key indole **8**. Deacetylation under acidic conditions gave the late-stage intermediate **9** which could then be converted to the final compounds by *N*-alkylation of the indole and aniline acylation – these steps may be carried out in either order.

Scheme 1. Synthesis of 2-Amino-5-phenoxyindole **11**.

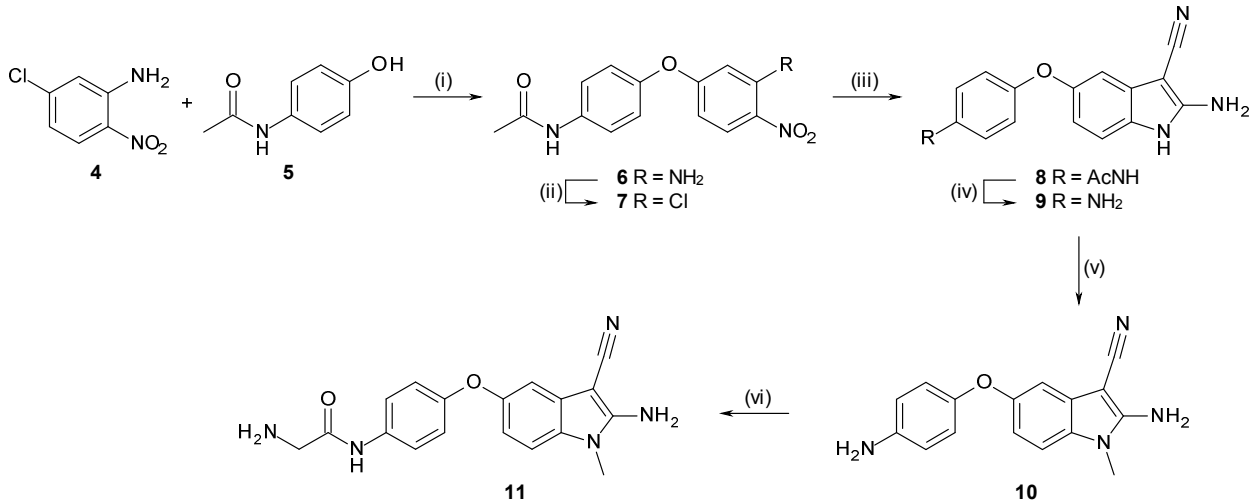

Reagents and conditions: (i) NaH, DMA, 5-80°C; (ii) *conc.* HCl, $NaNO_2$, H_2O, AcOH, CuCl, 5-50°C; (iii) malononitrile, NMP, 10M NaOH, room temperature; (iv) *conc.* HCl, MeOH, H_2O, 55°C; (v) MeI, Cs_2CO_3, DMF, 80-120°C. (vi) *N*-BOC-glycine, HATU, DCM, DIPEA, room temperature, then TFA, DCM, room temperature.

Deletion of the amino functionality from the indole required a different approach, illustrated for compound **26** (Scheme 2) which begins with the 3-cyanoindole **12.** Protection of the indole nitrogen with a 2-(trimethylsilyl)ethoxymethyl (SEM) protecting group followed by subsequent debenzylation using standard conditions yielded the 5-hydroxyindole **20** which could then be used in a subsequent S_NAr reaction to afford the nitro compound **21**. Reduction to aniline **22** was followed by amide formation to give doubly protected indole **23**. Selective removal of the SEM group allowed introduction of the alkyl indole *N*-substituent, with compound **26** then isolated after removal of the BOC protecting group.

Scheme 2. Synthesis of des-aminoindole **26**.

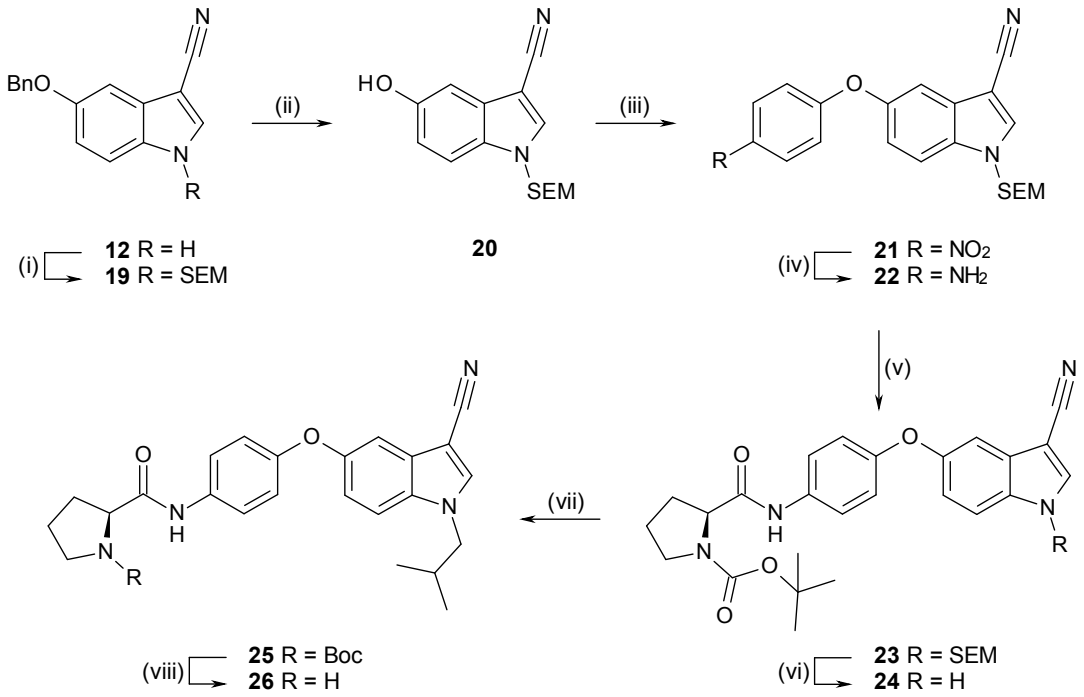

Reagents and conditions: (i) SEM-Cl, NaH, THF, 5-25°C; (ii) 10% Pd/C, H_2, MeOH, room temperature; (iii)1-

fluoro-4-nitrobenzene, K_2CO_3, DMF, room temperature; (iv) $NH_4^+Cl^-$, Zn, MeOH, room temperature; (v) Boc-Pro-OH, HATU, DMF, DIPEA, room temperature; (vi) TBAF, reflux; (vii) *i*-BuBr, Cs_2CO_3, DMF, room temperature; (viii) TFA, DCM, room temperature.

A scaffold change to the indazole series required the development of a different synthesis (Scheme 3) which involves diazotization of aniline **27** under standard conditions followed by cyclization to give indazole **28**. Protection of the indazole *NH* was similarly required prior to ether formation under copper catalyzed conditions to give **31** where the proline side chain was already installed. Similar deprotection and alkylation conditions to those used in the indole series were then employed to yield indazole **33**.

Scheme 3. Synthesis of indazole **33**.

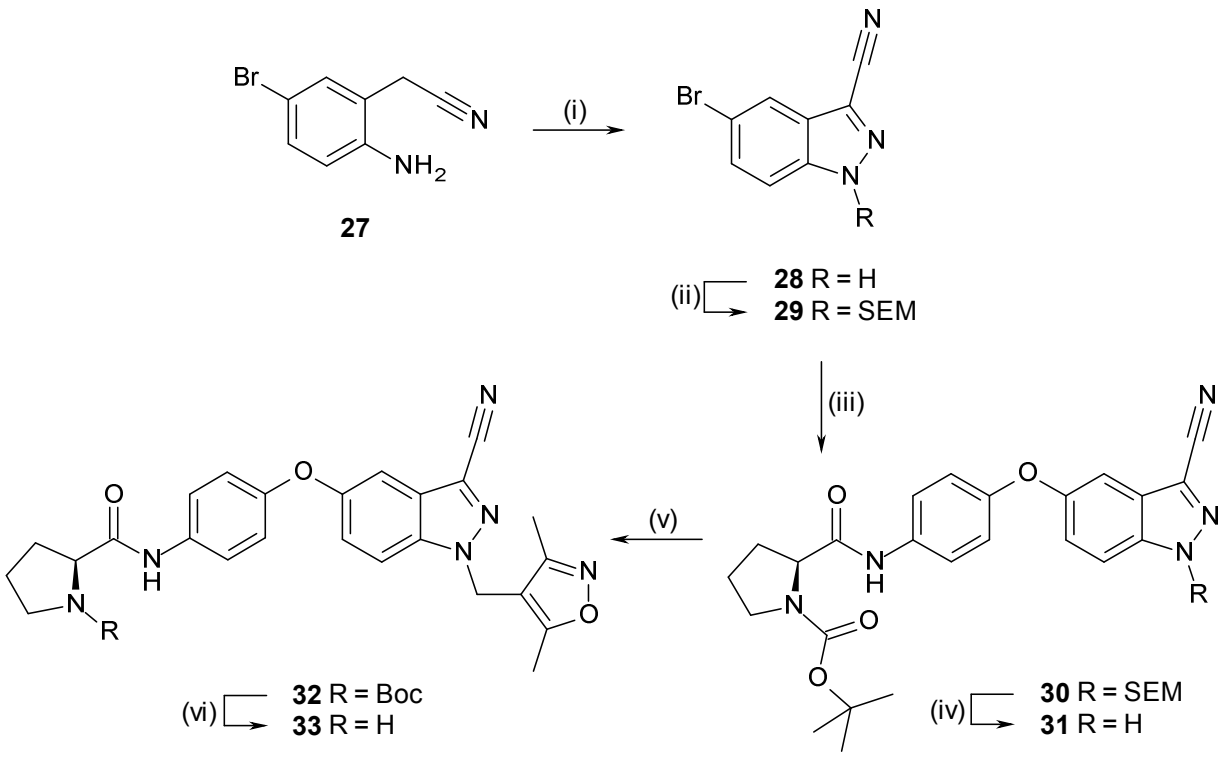

Reagents and conditions: (i) *conc.* HCl, $NaNO_2$, H_2O, -50-0°C; (ii) SEM-Cl, NaH, THF, -20-25°C; (iii) (*S*)-2-(4-hydroxy-phenylcarbamoyl)-pyrrolidine-1-carboxylic acid *tert*-butyl ester, CuI, Cs_2CO_3, *N*,*N*-dimethyl glycine HCl salt, DMF, 1,4-dioxane, 140°C; (iv) TBAF, 40°C; (v) 4-(chloromethyl)-3,5-dimethyl-isoxazole, NaH, THF, -5-25°C; (vi) TFA, DCM, room temperature.

Replacement of the indole nitrile group with *N*-methylpyrazole required the synthesis of a late stage bromo intermediate **38** which could then undergo a Suzuki coupling to introduce the required functionality (Scheme 4). 5-Hydroxyindole **34** was condensed with 4-fluoronitrobenzene to give phenoxy indole **35**. 3-Bromoindole **38** was obtained in a sequence involving reduction to aniline **36**, amide capping to give **37**, then bromination with NBS to yield **38**. Suzuki coupling and deprotection allowed access to target compound **40**. For synthesis of

N-methyl analogue **43**, the Suzuki coupling was conducted after prior methylation of the indole to give **41**.

Scheme 4. Synthesis of 3-pyrazole indoles **40** and **43**.

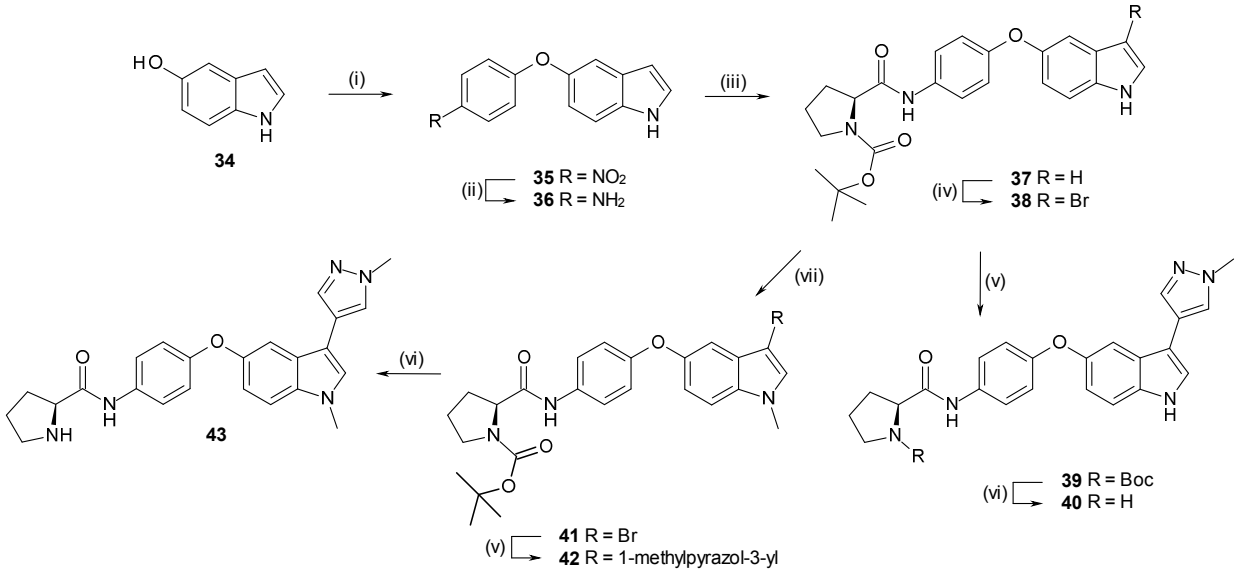

Reagents and conditions: (i)1-fluoro-4-nitrobenzene, Cs_2CO_3, DMF, room temperature; (ii) 10% Pd/C, H_2, MeOH, room temperature; (iii) Boc-Pro-OH, HATU, DMF, DIPEA, room temperature; (iv) NBS, DMF, room temperature. (v) 1-methyl-4-(4,4,5,5-tetramethyl-1,3,2-dioxaborolan-2-yl)pyrazole, $Pd(PPh_3)_4$, 1M K_3PO_4, 1,4-dioxane, 150°C; (vi) TFA, DCM, room temperature; (vii) MeI, Cs_2CO_3, DMF, room temperature.

RESULTS AND DISCUSSION

Screening of the AZ compound collection identified phenoxyindole **44** as a novel inhibitor of PFKFB3 with good selectivity over related isoforms PFKFB1 and 2 (Table 1). A crystal structure of **44** bound in the ATP pocket of PFKFB3 was solved and this highlighted several key interactions between ligand and enzyme (Figure 1). The indole occupies the adenosine binding

pocket sitting coplanar, and the phenoxy group occupies a lipophilic pocket and displaces water molecules seen when adenosine binds. Neither the nitrile nor the indole-2-amine appear to make any hydrogen bonds, although a water in the ribose pocket hydrogen bonds to the indole *NH*. Compared with the structure of ADP in complex with PFKFB3 there is a small amount of protein movement that allows the amide to bind, making a hydrogen bond between the amide amine and the backbone carbonyl oxygen of Leu238 (see Figure 2 for this interaction). The pocket for the amide tail is made accessible by protein movement, and although the electron density is not clear for this part of the molecule there are hydrophilic interactions available for the ligand. The pocket has polar side chains (His242 and Asn240) and a number of exposed backbone carbonyl oxygen and nitrogen atoms, and although the ligand does not interact directly with them these groups would be solvated and the ligand sits in this solvated environment. Residue Asn163 has also moved slightly relative to its position in the ADP structure. Subsequent testing of close analogues of **44** indicated key aspects of the SAR for this series. Compound **45**, the enantiomer of **44** was inactive, whereas deletion of the chiral alcohol side chain to give glycine amide **46** resulted in only a modest 4-fold drop in potency relative to **44**. This was perceived as an important result since it allowed us to dispense with one of seven hydrogen bond donors in **44**, features which may contribute to reduced permeability and increased efflux. Further deletion of the amino group in **46** to give acetamide **8** resulted in complete abrogation of activity illustrating the importance of this group. Although there are hydrophilic groups to interact with in this region, the amine does not appear to be held in a particularly tight hydrogen bonding network. Examination of the overlay of **44** with ATP indicated that the ribose pocket of ATP is not utilized by the inhibitor, but that alkylation of the indole nitrogen might allow access to this region of the enzyme. Alkylation with the progressively more lipophilic groups methyl, ethyl,

benzyl and isobutyl (compounds **11** and **48** through **50**) resulted in increasing potency against PFKFB3, with benzyl analogue **49** exhibiting greatest potency. These changes also had the consequence of increasing potency against PFKFB isoforms 1 and 2, although broadly, relative levels of selectivity versus PFKFB3 were maintained. A crystal structure of benzyl analogue **49** was solved in PFKFB3 highlighting an identical binding mode to that of **44**, with the benzyl ring directed into the ribose pocket although the phenyl ring does not directly overlay with the sugar moiety (Figure 2). The phenyl ring packs against Val234 making a hydrophobic interaction and Asn163 moves again compared to the structure with ADP and the structure of compound **49** overlays well with compound **44**, showing a consistent binding mode. Compound **50** which places a more hydrophilic acetamide group into the ribose pocket (logD = 0.5) shows a somewhat broader tolerance to groups in this region other than simple alkyl groups. Examination of these structures suggested no obvious role for the exocyclic indole-2-amino group in binding to the enzyme, and as highlighted we were concerned with the significant number of hydrogen bond donors present in the series. Gratifyingly, deletion of the amino group entirely had no significant impact on the observed levels of potency. Compounds **51** (des-amino analogue of **46**) and **52** (des-amino analogue of **47**) had, in each case, effectively equivalent levels of potency and isoform selectivity but for an increase in logD of 0.5 in each case. Selected compounds were assessed for evidence of inhibition of PFKFB3 in a cellular context. A549 cells (high expressers of PFKFB3) were treated with compound for 4 hours and then analyzed for a decrease in intracellular levels of F-1,6-BP by MSMS analysis, and for a decrease in secretion of lactate into the media. This assay also included an assessment of cytotoxicity to ensure that readouts were not adversely influenced by a cell-killing effect. Perhaps due to a combination of insufficient potency coupled with an excessive number of hydrogen bond donors potentially

limiting permeability, none of the compounds assayed in Table 1 showed target modulation in this assay. Compounds **48** and **49** showed no direct effect on F-1,6-BP levels but weak effects on lactate production which was associated with cell cytotoxicity. These two compounds both have high lipophilicity, and generally we observe effects on lactate production that are associated such cytotoxicity for most compounds with a logD above around 3.0.

Table 1. Cyanoindole inhibitors of PFKFB3 kinase

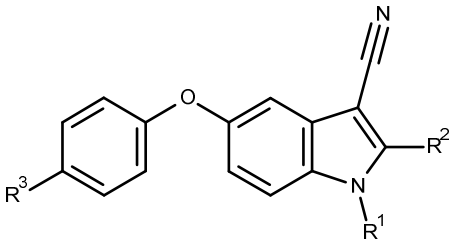

ID	R^1	R^2	R^3	PFKFB1 IC_{50}[a]	PFKFB2 IC_{50}[a]	PFKFB3 IC_{50}[a]	$logD_{7.4}$	Cell F-1,6-BP IC_{50}[b]	Cell Lactate IC_{50}[c]
44	H	NH_2	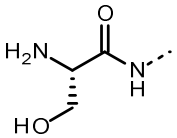	51.1	26.9	0.575	1.9	> 30	> 30
45	H	NH_2	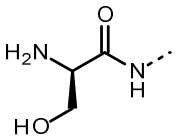	61.5	> 100	> 100	1.6		
46	H	NH_2	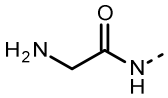	> 100	53.8	2.32	1.6		
8	H	NH_2	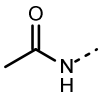	24.0	> 100	> 100	2.8		
11	Me	NH_2	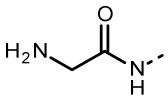	38.2	21.1	0.815	1.9		> 30

47	Et	NH_2	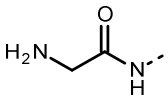	25.0	9.18	0.514	2.0	> 30	> 30
48	*i*-Bu	NH_2	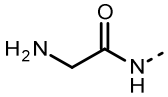	3.18	2.52	0.177	3.2	> 30	16.4[d]
49	Bn	NH_2	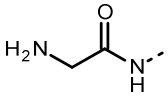	2.66	1.48	0.104	2.9	> 30	12.6[d]
50	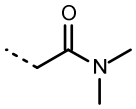	NH_2	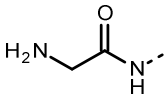	2.53	6.84	0.343	0.5	> 30	> 30
51	H	H	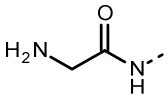	37.6	63.2	2.01	2.1		
52	Et	H	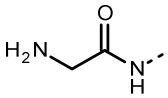	18.4	22.8	0.562	2.5		> 30

[a,b,c]All IC_{50} data are reported as micromolar and are the mean of at least n=2 independent measurements. Each has a SEM ± 0.2 log units. [b]Inhibition of fructose-1,6-bisphosphate in A549 cells. [c]Inhibition of lactate production in A549 cells. [d]Compounds show evidence of cytotoxicity in this assay.

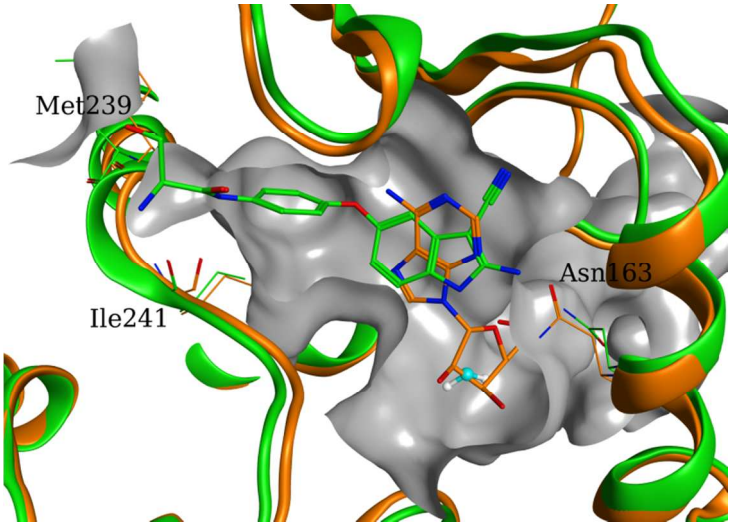

Figure 1. Crystal structure of **44** bound to the catalytic domain of PFKFB3 (shown in green, pdb code 5ajv), overlaid with the structure of PFKFB3 in complex with ADP (shown in orange, pdb code 2axn).

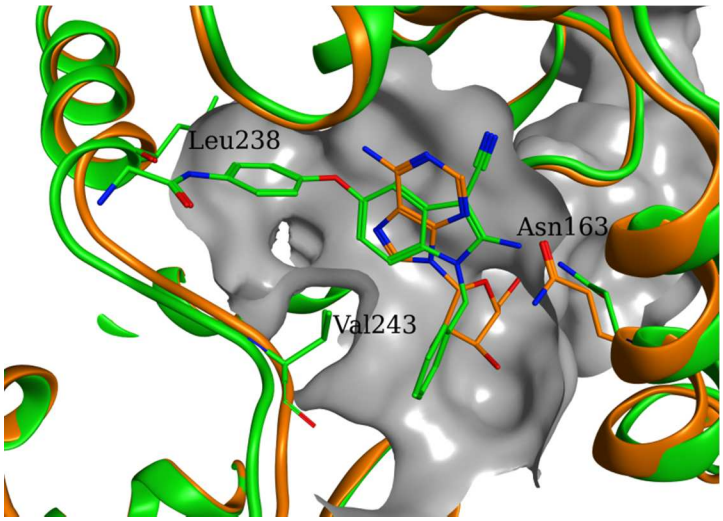

Figure 2. Crystal structure of **49** bound to the catalytic domain of PFKFB3 (shown in green, pdb code 5ajw), overlaid with the structure of PFKFB3 complexed with ADP (shown in orange, pdb code 2axn).

Table 2. Variations to the amino acid side chain

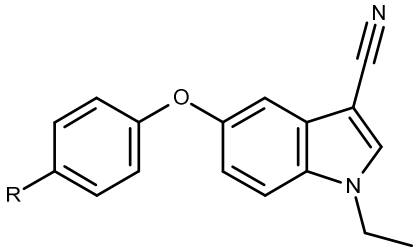

ID	R	PFKFB1 IC_{50}[a]	PFKFB2 IC_{50}[a]	PFKFB3 IC_{50}[a]	$logD_{7.4}$	Cell F-1,6-BP IC_{50}[b]	Cell Lactate IC_{50}[c]
53	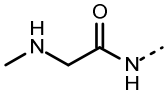	20.4	24.89	0.830	2.7		> 30
54	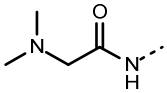	62.9	76.1	9.83			> 30
55	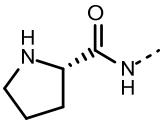	22.1	1.82	0.112	2.9	3.05	12.0
56	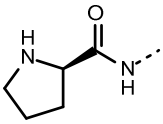	> 100	> 100	70.9	2.8		> 30
57	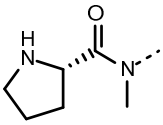	72.3	76.5	23.1	1.9		> 30
58	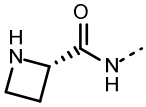	3.74	NT	0.086			19.6
59	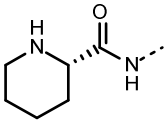	86.3	22.0	2.20	2.7		> 30
60	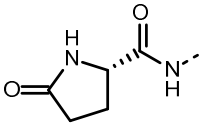	> 100	23.7	0.531	2.6		> 30

[a,b,c]All IC_{50} data are reported as micromolar and are the mean of at least n=2 independent measurements. Each has a SEM ± 0.2 log units. [b]Inhibition of fructose-1,6-bisphosphate in A549 cells. [c]Inhibition of lactate production in A549 cells.

Having observed relatively sharp SAR around the phenoxy amide tail in initial testing, we embarked on further specific modifications to this region, since the glycine tail was perceived to be a potential DMPK risk. Simple *N*-methylation of **52** to give **53** was tolerated with only a slight drop in potency for a slight increase in logD, but again removing one more hydrogen bond donor (Table 2). However exhaustive methylation to give dimethylamino substituted **54** caused a significant loss of potency indicating that at least one hydrogen bond donor was required for binding in this region. Capping of the pharmacophore with proline allowed ready access to a cyclized analogue of **53** in which the *N*-Me is conceptually tethered back onto the glycine side chain. Use of *S*-proline resulted in **55** which showed potent inhibition with an IC_{50} of 0.112 μM, although it is unclear if this gain in potency is a result of conformational restriction of the side chain, or simply due to the increased lipophilicity (logD = 2.9). This compound was the first to show appreciable on scale activity in the cell assay with an IC_{50} of 3 μM against the F-1,6-BP endpoint, and also activity against lactate secretion with no evidence of cellular toxicity. Compound **56**, synthesized using *R*-proline was completely inactive however, which is entirely consistent with the serine side chain enantiomeric preference seen in initial hits **44** and **45**. For the first time, the importance of the aromatic amide *NH* was illustrated by compound **57**, which is the methylated analogue of **55**. Methylation in this way resulted in over 200-fold loss in potency, to 23 μM due to removal of the key hydrogen bond between this amide NH and the carbonyl of Leu238 (see Figure 2). Further cyclic amino side chains were explored although again SAR appeared relatively narrow. Azetidine analogue **58** was the first analogue synthesized to breach 0.1 μM potency, although some stability issues were observed in handling of this group which precluded more detailed optimization. Expansion to a 6 membered ring of the preferred stereochemistry as in **59**, showed a 20-fold drop in potency relative to proline **55**. Final

confirmation that it was the presence of a donor that was required in this region, rather than simply a basic primary or secondary amino group, came in the form of lactam **60**. This neutral compound retained significant amounts of potency against PFKFB3.

Table 3. Optimization of the ribose pocket group

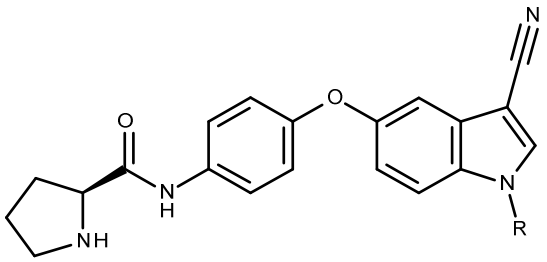

ID	R	PFKFB1 IC_{50}[a]	PFKFB2 IC_{50}[a]	PFKFB3 IC_{50}[a]	$logD_{7.4}$	Cell F-1,6-BP IC_{50}[b]	Cell Lactate IC_{50}[c]
26	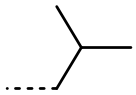	2.06	0.384	0.023	3.5	0.343	5.77[d]
61	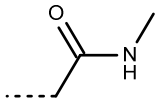	16.9	2.35	0.111	1.4	14.0	> 30
62	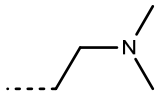	53.8	> 100	0.256	2.1	7.48	> 30
63	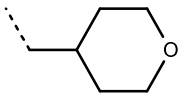	3.47	0.429	0.048	2.8	0.633	> 30
64	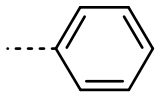	1.93	0.374	0.027	> 4.3		8.71[d]
65	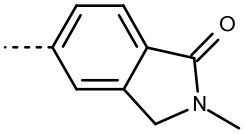	0.701	0.108	0.008	3.0	0.140	2.18

66	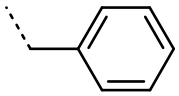	1.83	0.188	0.020	3.9		6.95[d]
67	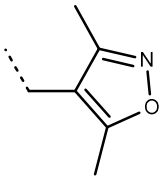	1.13	0.159	0.011	2.8	0.281	> 30

[a,b,c]All IC_{50} data are reported as micromolar and are the mean of at least n=2 independent measurements. Each has a SEM ± 0.2 log units. [b]Inhibition of fructose-1,6-bisphosphate in A549 cells. [c]Inhibition of lactate production in A549 cells. [d]Compounds show evidence of cytotoxicity in this assay.

Having optimized the phenoxy tail, we next revisited the indole *N*-substituent since in the earlier screening of analogues, this region had clearly been shown to impact potency most significantly. As previously observed, potent compounds could be obtained by appropriate use of lipophilic alkyl side chains, with isobutyl **26** demonstrating an IC_{50} of 0.023 μM (Table 3) and also having sub μM cellular activity albeit with some evidence of cytotoxicity due to the greater obersved lipophilicy (logD = 3.5). As potency against the primary target is enhanced, activity against the other isoforms also increases although a degree of selectivity is maintained. Typically across a wide range of compounds made, selectivity versus PFKFB2 was of the order of 10-fold, and 100-fold versus PFKFB1. Substituent tolerance in this position proved to be quite broad, with more polar examples such as amide **61**, bases as in **62**, and tetrahydropyran **63**, designed to more closely mimic the ribose group it replaces, all showing potent inhibition. Amide **61** showed weak cellular activity, likely due to a combination of weaker potency and additional hydrogen bond donor. Di-basic analogue **62** also had weaker cell activity in line with its enzyme potency. In addition to alkyl, direct aromatic linkers are also tolerated. Tetrahydropyran **63**, despite showing sub-micromolar activity against F-1,6-BP showed no activity against the more distal

lactate endpoint. *N*-Phenyl analogue **64** is a potent inhibitor of PFKFB3 and a variety of substituted aryl groups, including heterocycles are tolerated. The isoindolone compound **65** is representative of one of the more potent aromatic rings that can efficiently bind in the ribose pocket, with an IC_{50} of 8 nM, a level of activity that translated well to effects in the cell assay, with an IC_{50} of 140 nM, and low micromolar effects on lactate, with no evidence of cytotoxicity. Analogue **66** again contains a simple benzyl group directed to the ribose pocket and in comparison to the earlier incarnation in **49** is 5-fold more potent and with 3 fewer hydrogen bond donors. A wide variety of different benzylic groups could be tolerated in this region, including heterocyclic analogues such as isoxazole **67**, which also showed good activity in the cell assay, albeit with no apparent effects on lactate production. A crystal structure of **67** was obtained bound to PFKFB3 (Figure 3). The binding mode of compound **67** is identical to compound **49**. The basic amines both occupy the same space with a hydrogen bond to a conserved water molecule. Asn163 is disordered in this structure, suggesting the lack of an amine at the 2-position of the indole makes this side chain more flexible.

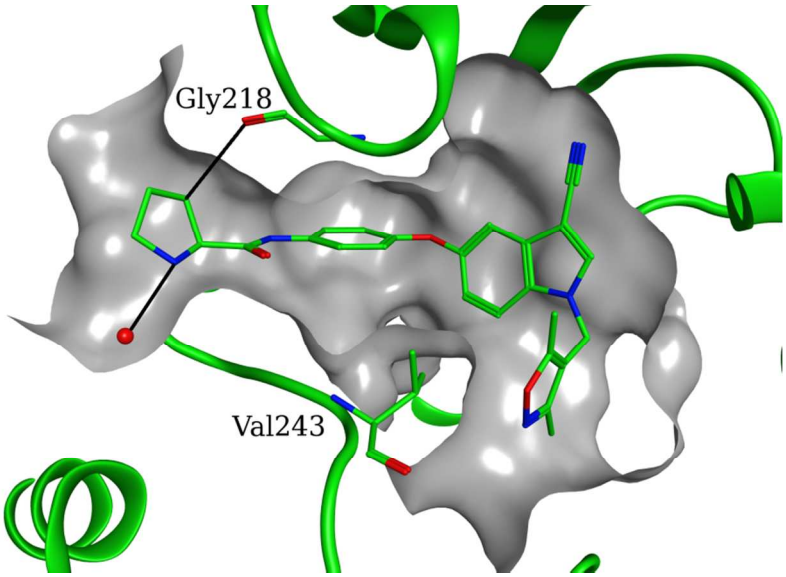

Figure 3. Crystal structure of **67** bound to the catalytic domain of PFKFB3 (pdb code 5ajx).

Table 4. Indazole analogues

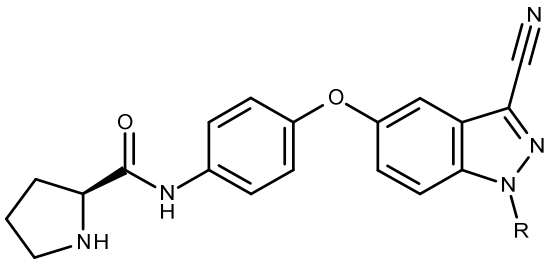

ID	R	PFKFB1 IC_{50}[a]	PFKFB2 IC_{50}[a]	PFKFB3 IC_{50}[a]	$logD_{7.4}$	Cell F-1,6-BP IC_{50}[b]	Cell Lactate IC_{50}[c]
68		0.294	0.015	0.004	3.6	0.297	15.4[d]
33	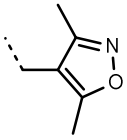	0.191	0.025	0.003	2.5	0.067	

[a,b,c]All IC_{50} data are reported as micromolar and are the mean of at least n=2 independent measurements. Each has a SEM ± 0.2 log units. [b]Inhibition of fructose-1,6-bisphosphate in A549 cells. [c]Inhibition of lactate production in A549 cells. [d]Compounds show evidence of cytotoxicity in this assay.

As part of the broader exploration of this template, we were motivated to synthesize indazole analogues **68** and **33**, which were exact matched pairs to potent indoles **26** and **67** respectively. Proximity of Asn163 to the indole *C*-2 position was noted, and offered the possibility of a hydrogen bonding interaction to *N*-2 of the corresponding indazole. Comparing *N*-isobutyl compounds **26** and **68**, the indazole gains around 5-fold potency for equivalent logD (IC_{50} improves to 0.004 μM from 0.023 μM), but notably, selectivity over the other isoforms is diminished (selectivity over PFKFB2 drops from 17-fold for the indole to less than 4-fold for

indazole). For isoxazole analogues **67** and **33** a similar pattern is observed, although it should be noted that at 0.003 μM, the potency of **33** is at the limit of the enzyme assay sensitivity and so absolute conclusions about changes in potency and selectivity are not possible. These improvements in enzyme potency also translated through into improved cellular activity with isoxazole substituted indazole analogue **33** showing the greatest cellular potency of all compounds in this study with an IC_{50} of 67 nM.

Table 5. Indoles with a flipped binding mode

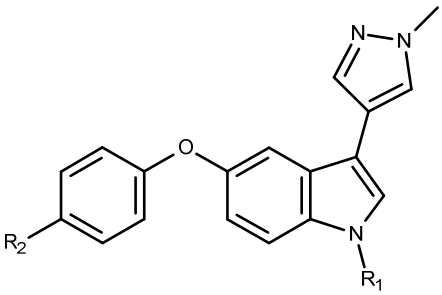

ID	R_1	R_2	PFKFB1 IC_{50}[a]	PFKFB2 IC_{50}[a]	PFKFB3 IC_{50}[a]	$logD_{7.4}$	Cell F-1,6-BP IC_{50}[b]	Cell Lactate IC_{50}[c]
69	H	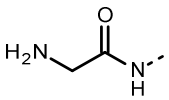	13.5	11.8	0.496	1.6	> 30	> 30
40	H	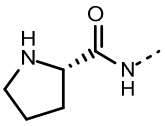	27.4	3.57	0.114	2.3	> 30	> 30
43	Me	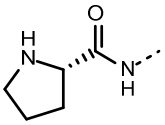	2.35	0.818	0.021	1.9	0.979	9.71

[a,b,c]All IC_{50} data are reported as micromolar and are the mean of at least n=2 independent measurements. Each has a SEM ± 0.2 log units. [b]Inhibition of fructose-1,6-bisphosphate in A549 cells. [c]Inhibition of lactate production in A549 cells.

The crystal structures generated to date had highlighted that the nitrile present in all analogues did not appear to form any specific interactions with the protein. In the course of exploration of alternatives to the nitrile, *N*-methylpyrazole **69** was synthesized as a direct analogue of earlier nitrile **51**, and this compound showed around a 4-fold improvement in potency relative to the nitrile but with lower lipophilicity (2.1 to 1.6). A crystal structure of **69** was obtained which highlighted an intriguing observation. Instead of acting as the nitrile mimic for which it was designed, the indole moiety was observed to flip through 180 degrees to allow binding of the pyrazole in the ribose pocket. Figure 4 shows the overlay of these two compounds and the subtle shift in small molecule architecture that allows this alternate binding mode, without appreciable change in the protein itself. The protein's binding site is slightly larger than the compounds in either binding mode, and along with the ability to maintain the hydrophobic interactions in both binding modes, the indoles can fit in either way round. Synthesis of the analogue with preferred proline solvent tail gave compound **40** which showed the anticipated improvement in potency in line with its increased lipophilicity. Since this new binding mode highlights the pocket previously occupied by the nitrile is empty, *N*-methylation was undertaken to give **43**, which showed a 5-fold increase in potency relative to **40**, with concomitant improvement in cellular activity despite a favourable drop in logD. Compound **43** shows around a 50-fold drop off between its enzyme potency and effects on F-1,6-BP modulation in cells, and a further 10-fold drop-off to effects on lactate secretion, with no evidence of cytotoxicity. Here again, a crystal structure determination of **43** revealed a most unexpected observation (Figure 5). The helix from Asp155 to Asn163 has rearranged, partially unwinding towards the *C*-terminus and forming a tighter alpha helix towards the *N*-terminus. This has an effect on the position of the side chains presenting towards the binding site, especially Val159. Interestingly the size and shape of the

binding site does not change much after this rearrangement, and both compounds fit comfortably into both binding sites. It is difficult to make a convincing explanation for this protein movement, and a subtle balance stabilizing the protein conformation with the binding energy will dictate the system's overall energy.

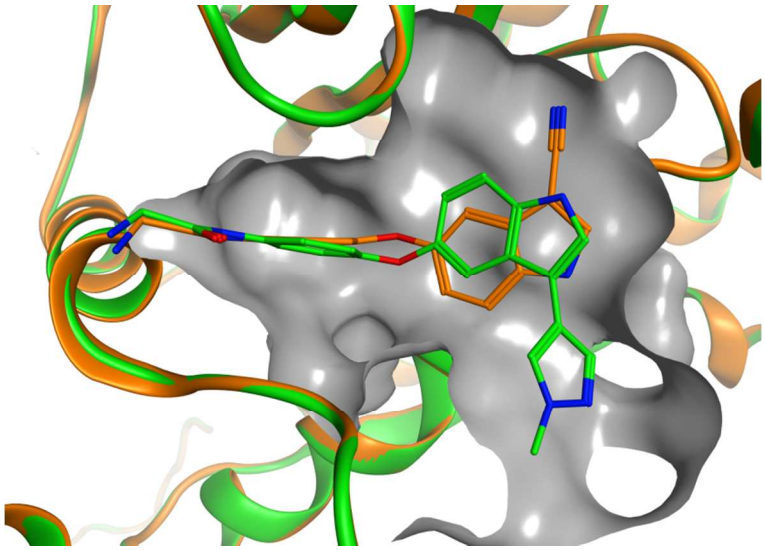

Figure 4. Crystal structure of **51** (orange, pdb code 5ajz) and **69** (green, pdb code 5ajy) overlaid in the catalytic domain of PFKFB3.

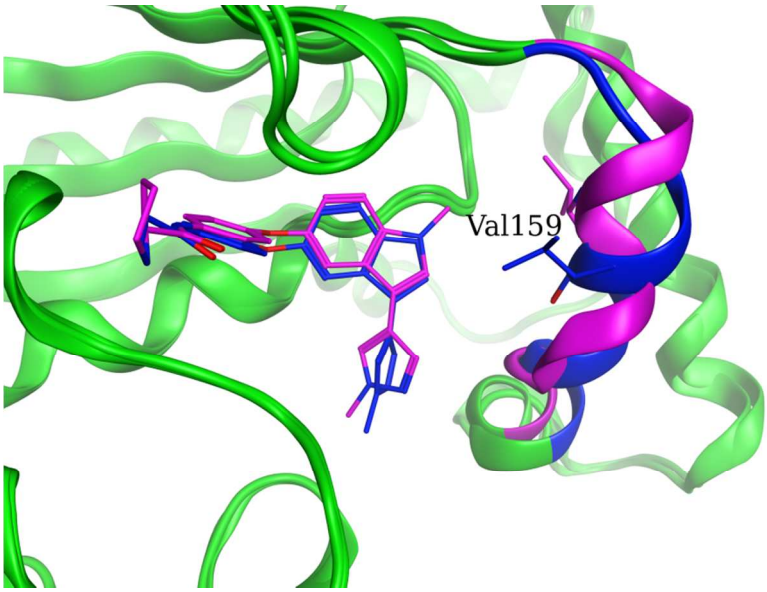

Figure 5. Crystal structure of **43** (blue, pdb code 5ak0) and **69** (magenta, pdb code 5ajy) overlaid in the catalytic domain of PFKFB3. The amino acids sequence from Asp155 to Asn163 are colored differently in each complex (compound **69** is colored magenta and compound **43** is colored blue) showing the difference between the two structures. Val159 is shown, highlighting the twist in location of this side chain.

Table 6. Changes to the linking atom

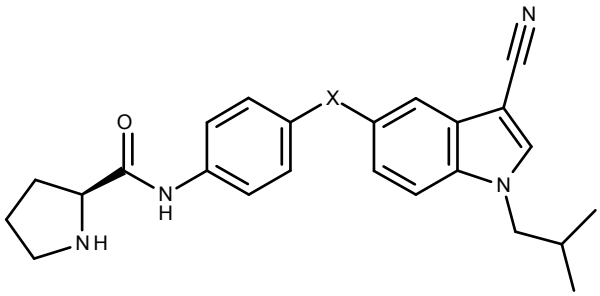

ID	X	PFKFB1 IC_{50}[a]	PFKFB2 IC_{50}[a]	PFKFB3 IC_{50}[a]	$logD_{7.4}$	Cell F-1,6-BP IC_{50}[b]	Cell Lactate IC_{50}[c]
26	O	2.06	0.384	0.023	3.5	0.343	5.77[d]
70	NH	36.6	6.15	1.57	2.7		> 30
71	NMe	5.0	0.141	0.075	3.8	> 30	13.7[d]
72	S	1.66	0.190	0.111	> 4.3		14[d]
73	SO_2	0.321	> 100	37.7	2.9	> 30	24.7
74	CH_2	5.92	1.45	0.199	3.9	> 30	> 30

[a,b,c]All IC_{50} data are reported as micromolar and are the mean of at least n=2 independent measurements. Each has a SEM ± 0.2 log units. [b]Inhibition of fructose-1,6-bisphosphate in A549 cells. [c]Inhibition of lactate production in A549 cells.

The impact of changing the heteroatom linker between phenyl and indole was also investigated (Table 6). A simple *NH* linker **70** (matched pair to *O*-linked **26**) lowered LogD but was poorly tolerated, showing a sharp drop in activity. However *N*-methylation as in **71** gave a profile comparable to O, albeit with increased lipophilicity. Weaker activity and higher lipophilicity was also a feature of *S*-linked analogue **72**. However, intriguingly when **72** was oxidized to sulfone **73**, a complete reversal of isoform selectivity was observed. This compound has an IC_{50} for PFKFB1 of 0.321 μM, and has selectivity of over 300- and 100-fold over PFKFB2 and 3 respectively. Finally, introduction of a methylene linker **74** saw a slight drop in PFKFB3 activity at greater lipophilicity penalty. Only the initial *O*-linked analogue demonstrated meaningful cellular effects however.

Compound **26** was selected for more detailed pharmacokinetic profiling (Table 7). Solubility is modest at 48 μM, and plasma protein binding is high in both rat and human, presumably linked to high lipophilicity. Mouse has lower levels of protein binding however. *In vitro* clearance in hepatocytes is remarkably consistent across all three species, with half lives in the range 21-28 minutes. When dosed to Wistar Han rats, **26** was observed to have very low *in vivo* clearance (although given high protein binding, unbound clearance is high), and high bioavailability, with a moderate half life of 3.4 h. In mouse, clearance was somewhat higher and bioavailability a more modest 42%, with a shorter half life of 1.4 h. In both species, the *in vivo* clearance is observed to correlate well with that predicted from the *in vitro* data, indicating that the primary clearance route *in vivo* is *via* hepatic metabolism. The fraction absorbed in both species is high and indicates that the absorption is driven by good solubility and high passive permeability, despite evidence in Caco2 cells that the compound is an efflux substrate. Good exposure was also

observed when **26** was dosed at a high dose of 124 μMol/kg to Nude mice, where an AUC of 259 μM.h and C_{max} of 35 μM were measured, indicating the potential for this compound to be an *in vivo* probe.

Table 7. Selected Pharmacokinetic parameters for compound **26**

Parameter	Value
Aqueous solubility $pH_{7.4}$	48 μM
pK_a (pyrrolidine)	8.1
Plasma protein binding % free (mouse, rat , human)	1.64, < 0.03, 0.33 %
Intrinsic hepatocyte clearance $t_{1/2}$ (mouse, rat , human)	21, 21, 28 mins
Caco2 intrinsic permeability Papp, $pH_{6.5}$	13.4 1E-6.cm/s
Caco2 efflux ratio	4.6
Bioavailability (mouse,[a] rat[b])	42, 100 %
Fraction absorbed (mouse,[a] rat[b])	0.6, 1.0
V_{ss} (mouse, rat)	3.3, 0.4 l/kg
Cl (mouse, rat)	38, 2 ml/min/kg
Predicted Cl (mouse, rat)[c]	26, 2 ml/min/kg
iv $t_{1/2}$ (mouse, rat)	1.4, 3.4 h

[a]PK parameters in CD1 mice when dosed po/iv at 2.5 μMol/kg. [b]PK parameters in 10-12 week old male Wistar Han rats (n=2) when dosed po at 3.1 μMol/kg and iv at 2.5 μMol/kg (formulation 5% DMSO, 95% Captisol (30% in water). [c]Clearance was predicted using intrinsic clearance measurements determined from fresh hepatocytes together with plasma protein binding assumed to be 0.01% free, using the well stirred model and an empirical correction factor derived in-house.

Compound **26** was also assessed in a large panel of externally available kinases assays in order to assess its selectivity, and therefore utility as a probe of PFKFB3 biology. When screened at a single concentration of 1 μM against a diverse panel of 267 kinases, **26** showed no significant

inhibition of any kinase (no kinase was inhibited at a level greater than 25%). This data is available as supplementary information.

CONCLUSIONS

A weak screening hit with suboptimal physicochemical properties was optimized against PFKFB3 kinase using critical structure-guided insights. Central to this optimization was progressive deletion of hydrogen bonding groups deemed to be non-essential for binding. Crystallographic studies highlighted binding at the ATP site, and featured a flexible helix that was able to shift in response to compound binding, and by appropriate substitution, a propensity for the ligand to flip in the active site was also observed. Unusually for a kinase inhibitor, despite binding in the ATP pocket, these compounds do not utilize the donor or acceptor interactions required by ATP itself. The resulting compounds demonstrated high selectivity over related PFKFB isoforms and potent modulation of the target in a cellular context, both in terms of direct impact on F-1,6-BP levels and weaker effects on lactate secretion. Potent examples were also able to demonstrate modulation of target and its pathway without undue effects on cell viability. The series disclosed here represents a novel hexose kinase inhibition template which as a consequence does not display appreciable kinase inhibition outside of the PFKFB3 family. A selected example demonstrated exposure in rodents following oral dosing. Examples from this series may serve as useful probes to understand the emerging biology of this interesting metabolic target, in particular to expand upon the mostly biological si/shRNA validation undertaken to date.

ACKNOWLEDGMENTS

We would like to thank Ian Sinclair for helpful chromatography support in development of the cell assay.

AUTHOR INFORMATION

Corresponding Author

*Phone: +44 (0)1625 517920. Email: jason.kettle@astrazeneca.com.

Experimental Methods

Chemistry Unless otherwise stated, commercially available reagents were used as supplied. All reactions requiring anhydrous conditions were conducted in dried apparatus under an atmosphere of nitrogen. ^{1}H NMR spectra were recorded using a Bruker AV400 or AV500 NMR. Chemical shifts δ are reported in ppm and multiplicity of signals are denoted s = singlet, d = doublet, t = triplet and m = multiplet respectively, with coupling constants (*J*) reported in hertz (Hz). HRMS were recorded using a Thermo Accela CTC - LTQ FT instrument (ESI+). Reactions and intermediates were also characterised by mass spectroscopy following liquid chromatography (LCMS or UPLC); UPLC was carried out using a Waters UPLC fitted with Waters SQ mass spectrometer (Column temp 40, UV = 220-300 nm, MS = ESI with pos/neg switching) at a flow rate of 1ml/min using a solvent system of 97% A + 3% B to 3% A to 97% B over 1.50 minutes (total runtime with equilibration back to starting conditions etc 1.70min), where A = 0.1% Formic acid in water (for acid work) or 0.1% Ammonia in water (for base work) B = Acetonitrile. For acid analysis the column used was Waters Acquity HSS T3 1.8um 2.1 x 50 mm, for base analysis the column used was Waters Acquity BEH 1.7um 2.1 x 50mm. LCMS was

carried out using a Waters Alliance HT (2795) fitted with a Waters ZQ ESCi mass spectrometer and a Phenomenex Gemini –NX (50x2.1 5um) column at a flow rate of 1.1mL/min 95% A to 95% B over 4 min with a 0.5 min hold. The modifier is kept at a constant 5% C (50:50 acetonitrile:water 0.1% Formic acid) or D (50:50 acetonitrile:water 0.1% ammonium hydroxide (0.88 SG) depending on whether it is an acidic or basic method. Ion exchange purification was generally performed using a SCX-2 (Biotage, Propylsulfonic acid functionalized silica. Manufactured using a trifunctional silane. Non end-capped) cartridge. Individual purification methods referred to here are detailed in the Supplementary section.

***N*-[4-(3-Amino-4-nitro-phenoxy)phenyl]acetamide (6).** *N*-(4-Hydroxy-phenyl)-acetamide **5** (1.14 g, 6.62 mmol) was stirred in DMA (10 mL) and the mixture was cooled to 5°C under an atmosphere of nitrogen. Sodium hydride (60% dispersion in oil, 0.26 g, 6.62 mmol) was added portionwise over 10 minutes. The reaction mixture was allowed to warm to room temperature and stirred for 1 hour. 5-Chloro-2-nitro-phenylamine **4** (1 g, 6.615 mmol) was added in one portion and the mixture was heated to 80°C overnight. The mixture was cooled on an ice/water bath and then poured into 2M HCl (100 mL) before being extracted into ethyl acetate (200 mL). The organic layer was washed with water (3 x 200 mL) then brine (100 mL) before being dried ($MgSO_4$) and evaporated to afford a brown solid. The crude product was triturated with DCM to afford **6** (1.1 g, 58%). LCMS (ES^+) 288.21 $(M+H)^+$. ^1H NMR δ (d^6-DMSO) 10.05 (br s, 1H), 7.99 (d, J = 9.2Hz, 1H), 7.67 (d, J = 9.0Hz, 2H), 7.47 (br s, 2H), 7.11 (d, J = 9.0Hz, 2H), 6.26 – 6.32 (m, 2H), 2.06 (s, 3H).

***N*-[4-(3-Chloro-4-nitro-phenoxy)-phenyl]-acetamide (7).** *N*-[4-(3-amino-4-nitro-phenoxy)phenyl]acetamide **6** (1.10 g, 3.83 mmol) was added to a mixture of concentrated HCl (15 mL), water (25 mL) and acetic acid (20 mL). The mixture was cooled to 5°C and sodium nitrite (0.26 g, 3.83 mmol) was added dropwise. The reaction mixture was stirred for 15 minutes then copper chloride (0.42 g, 4.21 mmol) was added in portions - vigorous effervescence and a mild exotherm was observed. After heating to 50°C and being stirred for 30 minutes the mixture was cooled and extracted into ethyl acetate (2 x 100 mL). The organic layer was washed with water (3 x 200 mL) then brine (100 mL) before being dried ($MgSO_4$) and evaporated to afford crude product which was purified by flash silica chromatography, elution gradient 30 to 70% ethyl acetate in cyclohexane to afford **7** (0.8 g, 68%) as a yellow solid. LCMS (ES^+) 307.15 $(M+H)^+$. ^1H NMR δ ($CDCl_3$) 7.97 (d, *J* = 8.8Hz, 1H), 7.58 (d, *J* = 8.8Hz, 2H), 7.22 (br s, 1H), 7.08 - 7.03 (m, 3H), 6.91 (dd, *J* = 9.2Hz, 2.8Hz, 1H), 2.21 (s, 3H).

***N*-[4-(2-Amino-3-cyano-1*H*-indol-5-yloxy)-phenyl]-acetamide (8).** *N*-[4-(3-Chloro-4-nitro-phenoxy)-phenyl]-acetamide **7** (2.00 g, 6.52 mmol) and malononitrile (0.43 g, 6.52 mmol) were dissolved in NMP (30 mL) and 10M NaOH (1.30 mL) was added dropwise. The temperature rose to 30°C. The reaction mixture was stirred at room temperature for 16 hours before being diluted with DMF (20 mL). A solution of sodium bicarbonate (4 g) in water (25 mL) was added in portions (exotherm). The mixture was then allowed to cool to room temperature before sodium dithionite (10 g, 57 mmol) was added in portions followed by sodium bicarbonate (4 g) in water (25 mL). The mixture was allowed to stir at room temperature overnight. The resulting dark red suspension was partitioned between ethyl acetate (100 mL) and water (100 mL) and the organic layer was washed with water (3 x 100 mL) then brine (50 mL) before being dried ($MgSO_4$) and evaporated to afford a dark brown oil which was triturated with DCM/ethyl acetate

(10:1 mixture) to afford **8** (1.30 g, 65%) as a light brown oily solid. HRMS ESI+ *m/z* observed 307.1205, $C_{17}H_{15}N_4O_2$ requires 307.1195. ^{1}H NMR δ (d6-DMSO) 10.62 (br s, 1H), 9.81 (s, 1H), 7.45 (d, *J* = 9.0Hz, 2H), 7.02 (d, *J* = 8.4Hz, 1H) 6.82 (d, *J* = 9.0Hz, 2H), 6.73 (br s, 2H), 6.58 (d, *J* = 2.3Hz, 1H), 6.51 (dd, *J* = 8.4Hz, 2.3Hz, 1H), 1.94 (s, 3H).

2-Amino-5-(4-amino-phenoxy)-1*H*-indole-3-carbonitrile (9). *N*-[4-(2-Amino-3-cyano-1*H*-indol-5-yloxy)-phenyl]-acetamide **8** (1.30 g, 4.24 mmol) was stirred in methanol (40 mL)/water (8 mL) and concentrated HCl (4 mL) was added. The mixture was heated to 55°C for 16 hours before being partitioned between ethyl acetate (100 mL) and water (100 mL). The organic layer was dried ($MgSO_4$) and evaporated then purified by flash silica chromatography, elution gradient 50% to 100% ethyl acetate in cyclohexane to afford **9** (0.65 g, 58%) as a light yellow solid. LCMS (ES^+) 265.19 $(M+H)^+$. ^{1}H NMR δ (d^6-DMSO) 10.60 (s, 1H), 7.03 (dd, *J* = 7.9Hz, 1.0Hz, 1H), 6.75 (br s, 2H) 6.72 (d, *J* = 8.8Hz, 2H), 6.56 (d, *J* = 8.8Hz, 2H), 6.54 – 6.50 (m, 2H), 4.89 (br s, 2H).

2-Amino-5-(4-amino-phenoxy)-1-methyl-1*H*-indole-3-carbonitrile (10). 2-Amino-5-(4-amino-phenoxy)-1*H*-indole-3-carbonitrile **9** (0.1 g, 0.38 mmol) was dissolved in DMF (3 mL) and caesium carbonate (0.15 g, 0.46 mmol) was added followed by iodomethane (23 µL, 0.38 mmol). The mixture was stirred at room temperature for 3 hours before being evaporated then partitioned between DCM (3 mL) and water (3 mL). The organic layer was dried ($MgSO_4$) and evaporated then purified by flash silica chromatography, elution gradient 20% to 60% ethyl acetate in cyclohexane to afford impure product as a clear oil. Purification by prep LCMS (Method B) afforded **10** (32 mg, 27%) as a white solid. LCMS (ES^+) 279.33 $(M+H)^+$. ^{1}H NMR δ (d^6-DMSO) 7.14 (d, *J* = 8.4Hz, 1H), 6.98 (s, 2H), 6.72 (d, *J* = 8.8Hz, 2H), 6.61 - 6.54 (m, 4H), 4.91 (br s, 2H), 3.48 (s, 3H).

2-Amino-*N*-[4-(2-amino-3-cyano-1-methyl-1*H*-indol-5-yloxy)-phenyl]-acetamide (11). 2-Amino-5-(4-amino-phenoxy)-1-methyl-1*H*-indole-3-carbonitrile **10** (30 mg, 0.11 mmol) was suspended in DCM (2 mL) and *N*-(*tert*-butoxycarbonyl)glycine (29 mg, 0.16 mmol) was added followed by *N,N,N′,N′*-tetramethyl-*O*-(1*H*-benzotriazol-1-yl)uronium hexafluorophosphate (81 mg, 0.28 mmol) and diisopropylethylamine (37 µL, 0.21 mmol). The mixture was stirred at room temperature overnight before being evaporated. The residue was dissolved in DCM (1 mL) and TFA (1 mL) was added and the mixture was stirred at room temperature for 1 h. The reaction mixture was evaporated then purified by prep LCMS (Method B) then free based by absorbing onto a 1 g SCX cartridge, washing with methanol then eluting with 2M ammonia in methanol. Fractions containing desired product were evaporated under a stream of nitrogen then in a vacuum oven at 40°C for 16 hours to afford **11** (11 mg, 31%) as a white solid. HRMS ESI+ *m/z* observed 336.1460, $C_{18}H_{17}N_5O_2$ requires 336.1460. ^{1}H NMR δ (d^6-DMSO) 7.68 (d, *J* = 9.0Hz, 2H), 7.30 (d, *J* = 8.5Hz, 1H), 7.14 (br s, 2H), 7.00 (d, *J* = 9.0Hz, 2H), 6.79 (d, *J* = 2.1Hz, 1H), 6.75 (dd, *J* = 8.5Hz, 2.1Hz, 1H), 3.59 (s, 3H), 3.34 (s, 2H). Amide NH and NH_2 not observed.

5-Benzyloxy-1-(2-trimethylsilylethoxymethyl)indole-3-carbonitrile (19). 5-Benzyloxy-1*H*-indole-3-carbonitrile **12** (3 g, 12.08 mmol) was dissolved in THF (80 mL) and the mixture was cooled to 5°C under a nitrogen atmosphere. Sodium hydride (0.6 g, 15.1 mmol) was added in portions then the mixture was stirred at 5°C for 15 minutes. 2-(Chloromethoxy)ethyl-trimethyl-silane (2.35 mL, 13.29 mmol) was added and the mixture was allowed to warm to room temperature and stirred for 1 hour. The reaction was quenched by cautious addition of water then partitioned between water (500 mL) and ethyl acetate (300 mL). The organic layer was dried ($MgSO_4$) and evaporated then purified by flash silica chromatography, elution gradient 0% to 20% ethyl acetate in cyclohexane to afford **19** (2.9 g, 63%) as an off-white solid. LCMS (ES$^+$)

379.23 $(M+H)^+$. ^{1}H NMR δ ($CDCl_3$) 7.68 (s, 1H), 7.55 – 7.38 (m, 6H), 7.32 (d, *J* = 2.3Hz, 1H), 7.13 (dd, *J* = 9.0Hz, 2.3Hz, 1H), 5.51 (s, 2H), 5.18 (s, 2H), 3.52 (t, *J* = 8.1Hz, 2H), 0.91 (t, *J* = 8.1Hz, 2H), -0.05 (s, 9H).

5-Hydroxy-1-(2-trimethylsilylethoxymethyl)indole-3-carbonitrile (20). 5-Benzyloxy-1-(2-trimethylsilylethoxymethyl)indole-3-carbonitrile **19** (2.9 g, 7.66 mmol) was dissolved in methanol (40 mL) and the solution was added to 10% palladium on charcoal (100 mg) under nitrogen. The mixture was evacuated and flushed with nitrogen (x 3) then evacuated and flushed with hydrogen (x 3). The reaction mixture was then stirred under hydrogen at atmospheric pressure for 1 hour before filtering through celite and evaporating to yield crude product. The crude product was purified by flash silica chromatography, elution gradient 10% to 30% ethyl acetate in cyclohexane to afford **20** (1.45 g, 66%) as a white solid. LCMS (ES^+) 289.29 $(M+H)^+$. ^{1}H NMR δ (d6-DMSO) 9.37 (s, 1H), 8.28 (s, 1H), 7.50 (d, *J* = 8.9Hz, 1H), 6.91 (d, *J* = 2.3Hz, 1H), 6.84 (dd, *J* = 8.9Hz, 2.3Hz, 1H), 5.54 (s, 2H), 3.44 (t, 7.9Hz, 2H), 0.81 (t, *J* = 7.9Hz, 2H), -0.10 (s, 9H).

5-(4-Nitrophenoxy)-1-(2-trimethylsilylethoxymethyl)indole-3-carbonitrile (21). 5-Hydroxy-1-(2-trimethylsilylethoxymethyl)indole-3-carbonitrile **20** (1.45 g, 5.03 mmol), 1-fluoro-4-nitro-benzene (0.71 g, 5.03 mmol) and potassium carbonate (1.37 g, 10.06 mmol) were stirred in DMF (20 mL) at room temperature overnight. The reaction mixture was partitioned between ethyl acetate (200 mL) and water (200 mL) then the organic layer was dried ($MgSO_4$) and evaporated. The crude product was purified by flash silica chromatography, elution gradient 0% to 20% ethyl acetate in cyclohexane to afford **21** (1.84 g, 89%) as a yellow oil. LCMS (ES^+) 410.33 $(M+H)^+$. ^{1}H NMR δ (d^6-DMSO) 8.54 (s, 1H), 8.25 (d, *J* = 9.2Hz, 2H), 7.85 (d, *J* = 8.9Hz, 1H), 7.48 (d, *J*

= 2.3Hz, 1H), 7.23 (dd, *J* = 8.9Hz, 2.3Hz, 1H), 7.11 (d, *J* = 9.2Hz, 2H), 5.67 (s, 2H) , 3.53 (t, *J* = 7.9Hz, 2H), 0.84 (t, *J* = 7.9Hz, 2H), -0.07 (s, 9H).

5-(4-Aminophenoxy)-1-(2-trimethylsilylethoxymethyl)indole-3-carbonitrile (22). 5-(4-Nitrophenoxy)-1-(2-trimethylsilylethoxymethyl)indole-3-carbonitrile **21** (1.84 g, 4.49 mmol) was dissolved in DCM (20 mL)/methanol (20 mL) and ammonium chloride (2.4 g, 44.93 mmol) was added followed by zinc (2.35 g, 35.95 mmol). The mixture was stirred at room temperature overnight and then filtered through celite, washed with DCM/methanol (20 mL) then evaporated. The residue was partitioned between ethyl acetate (100 mL) and water (100 mL) then the organic layer was dried ($MgSO_4$) and evaporated to afford **22** (1.78 g, 104%) as an orange oil. LCMS (ES^+) 380.41 $(M+H)^+$. ^1H NMR δ (d^6-DMSO) 8.48 (s, 1H), 7.75 (d, *J* = 9.0Hz, 1H), 7.12 (dd, *J* = 9Hz, 2.4Hz, 1H), 7.00 (d, *J* = 2.4Hz, 1H), 6.87 (d, *J* = 8.8Hz, 2H), 6.69 (d, *J* = 8.8Hz, 2H), 5.58 (s, 2H), 4.97 (s, 2H), 3.45 (t, 7.9Hz, 2H), 0.81 (t, *J* = 7.9Hz, 2H), -0.10 (s, 9H).

***tert*-Butyl (2*S*)-2-[[4-[3-cyano-1-(2-trimethylsilylethoxymethyl)indol-5-yl]oxyphenyl]carbamoyl]pyrrolidine-1-carboxylate (23).** 5-(4-Aminophenoxy)-1-(2-trimethylsilylethoxymethyl)indole-3-carbonitrile **22** (1.0 g, 2.63 mmol), (2*S*)-1-*tert*-butoxycarbonylpyrrolidine-2-carboxylic acid (0.68 g, 3.16 mmol), *N,N,N′,N′*-tetramethyl-*O*-(1*H*-benzotriazol-1-yl)uronium hexafluorophosphate (1.5 g, 3.95 mmol) and diisopropylethylamine (0.92 mL, 5.27 mmol) were stirred in DCM (20 mL) for 16 hours. The reaction mixture was diluted with DCM (100 mL) then washed with water (100 mL). The organic layer was dried ($MgSO_4$) and evaporated then purified by flash silica chromatography, elution gradient 10% to 40% ethyl acetate in cyclohexane to afford **23** (1.05 g, 69%) as a white solid. LCMS (ES^+) 577.48 $(M+H)^+$. ^1H NMR δ (d^6-DMSO) 10.07 (br s, 1H), 8.53 (s, 1H), 7.83 (m, 1H), 7.68 (d, *J* = 8.9Hz, 2H), 7.19 (m, 2H), 7.07 (d, *J* = 8.9Hz, 2H), 5.61 (s, 2H), 4.19 (m, 1H), 3.48 (t, *J* = 7.8Hz,

2H), 3.39 (m, 1H), 2.95 (br s, 1H), 2.18 (m, 1H), 1.95 – 1.70 (m, 3H), 1.39 (s, 9H), 0.82 (t, *J* = 7.8Hz, 2H), -0.09 (s, 9H).

***tert*-Butyl (2*S*)-2-[[4-[(3-cyano-1*H*-indol-5-yl)oxy]phenyl]carbamoyl]pyrrolidine-1-carboxylate (24).** *tert*-Butyl (2*S*)-2-[[4-[3-cyano-1-(2-trimethylsilylethoxymethyl)indol-5-yl]oxyphenyl]carbamoyl]pyrrolidine-1-carboxylate **23** (1.05 g, 1.82 mmol) was dissolved in THF (10 mL) and tetrabutylammonium fluoride, 1M solution in THF (1.82 mL, 1.82 mmol) was added and the mixture was heated at reflux for 16 hours. The reaction was incomplete so a further portion of tetrabutylammonium fluoride, 1M solution in THF (1.82 mL, 1.82 mmol) was added and the mixture was heated at reflux for a further 7 hours before cooling to room temperature. After standing for 72 hours the mixture was partitioned between ethyl acetate (100 mL) and water (100 mL). The organic layer was washed with water (100 mL) then dried ($MgSO_4$) and evaporated to afford **24** (0.76 g, 93%) as a white solid. LCMS (ES^+) 447.40 $(M+H)^+$. ^1H NMR δ (d^6-DMSO) 12.25 (br s, 1H), 9.97 (s, 1H), 8.25 (s, 1H), 7.62 – 7.54 (m, 3H), 7.09 (m, 1H), 7.03 – 6.95 (m, 3H), 4.27 – 4.13 (m, 1H), 3.42 (m, 1H), 2.20 (m, 1H), 1.95 – 1.75 (m, 3H), 1.40 (s, 3H), 1.28 (s, 6H), 0.96 – 0.84 (m, 1H).

(2*S*)-*N*-[4-[3-Cyano-1-[2-(methylamino)-2-oxo-ethyl]indol-5-yl]oxyphenyl]pyrrolidine-2-carboxamide (26). *tert*-Butyl (2*S*)-2-[[4-[(3-cyano-1*H*-indol-5-yl)oxy]phenyl]carbamoyl]pyrrolidine-1-carboxylate **24** (50 mg, 0.11 mmol) was dissolved in DMF (1 mL) and cesium carbonate (55 mg, 0.17 mmol) was added followed by 1-bromo-2-methyl-propane (0.012 mL, 0.11 mmol). The reaction mixture was stirred at room temperature for 16 hours before being partitioned between water (10 mL) and ethyl acetate (10 mL). The organic layer was washed with water (2 x 10 mL), brine (10 mL) and then dried ($MgSO_4$) and evaporated. The residue was then taken up in DCM (1 mL) and treated with TFA (1 mL) and

stirred at room temperature for 30 minutes. The reaction mixture was evaporated then purified by prep LCMS (Method A) then free-based by absorbing onto a 1 g SCX cartridge, washing with methanol then eluting with 2M ammonia in methanol. Fractions containing the desired product were evaporated under a stream of nitrogen then in a vacuum oven at 40°C overnight to afford **26** (26 mg, 58%) as a white solid. HRMS ESI+ *m/z* observed 403.21301, $C_{24}H_{27}N_4O_2$ requires 403.21285. ^{1}H NMR δ (d^6-DMSO) 9.99 (s, 1H), 8.30 (s, 1H), 7.73 (d, *J* = 8.9Hz, 1H), 7.67 (d, *J* = 9.0Hz, 2H), 7.08 (d, *J* = 2.2Hz, 1H), 7.06 (dd, *J* = 8.9Hz, 2.2Hz, 1H), 6.99 (d, *J* = 9.0Hz, 2H), 4.07 (d, *J* = 7.4Hz, 2H), 3.72 (m, 1H), 3.00 (br s, 1H), 2.91 (t, *J* = 6.6Hz, 2H), 2.20 – 2.00 (m, 2H), 1.83 – 1.73 (m, 1H), 1.70 – 1.62 (m, 2H), 0.85 (d, *J* = 6.6Hz, 6H).

5-Bromo-1*H*-indazole-3-carbonitrile (28). 2-(2-Amino-5-bromo-phenyl)acetonitrile **27** (1.25 g, 5.92 mmol) was dissolved in concentrated aq. HCl (20 mL) and cooled to -50°C (partial solidification observed). To this mixture was added a solution of $NaNO_2$ (516 mg, 7.48 mmol) in water (2.5 mL) dropwise over 20 minutes. The reaction mixture was stirred for a further 1 hour at -50°C, before gradually warming to 0°C and then made basic by the careful addition of 35% aq. ammonia (35 mL). After warming to room temperature, the solution was extracted with ethyl acetate (3 x 80 mL), the combined organic layers were washed with brine, dried (filtered though a phase separator paper) and evaporated to give 3.2 g crude solid. The product was purified by flash silica chromatography, elution gradient 0% to 20% ethyl acetate in cyclohexane to afford **28** (1.19 g, 91%) as a white solid. LCMS (ES^+) 221.95/223.99 (M+H). ^{1}H NMR δ (d^6-DMSO) 14.58 (br s, 1H), 8.17 (dd, *J* = 1.8, 0.7 Hz, 1H), 7.76 (dd, *J* = 8.9, 0.7 Hz, 1H) 7.67 (dd, *J* = 8.9, 1.8 Hz, 1H).

5-Bromo-1-(2-trimethylsilylethoxymethyl)indazole-3-carbonitrile (29). To a stirred soln of 5-bromo-1*H*-indazole-3-carbonitrile **28** (1.19 g 5.36 mmol) in anhydrous THF (30 mL) under

nitrogen at -20°C was added NaH (60% in mineral oil, 257 mg, 6.43 mmol). The mixture was stirred for 40 minutes, then 2-(chloromethoxy)ethyl-trimethyl-silane (1.05 mL, 5.91 mmol) was added dropwise. The mixture was stirred at -20°C for a further 45 minutes then warmed to room temperature and left stirring for a further 30 minutes. Water (10 mL) was added, then the mixture was concentrated before adding more water (100 mL). The mixture extracted with ethyl acetate (2 x 100 mL) and the combined organic layers were washed with brine, dried (filtered though a phase separator paper) and evaporated to give **29** (1.89 g, 100%) as an orange solid. LCMS (ES^+) M+H not found. ^{1}H NMR δ ($CDCl_3$): 8.04 (dd, *J* = 1.6, 0.8 Hz, 1H), 7.64 (dd, *J* = 8.9, 1.6 Hz, 1H), 7.60 (dd, *J* = 8.9, 0.8 Hz, 1H), 5.77 (s, 2H), 3.55 (t, *J* = 8.3 Hz, 2H), 0.89 (t, *J* = 8.3 Hz, 2H), -0.05 (s, 9H).

tert-Butyl (2*S*)-2-[[4-[3-cyano-1-(2-trimethylsilylethoxymethyl)indazol-5-yl]oxyphenyl]carbamoyl]pyrrolidine-1-carboxylate (30). 5-Bromo-1-(2-trimethylsilylethoxymethyl)indazole-3-carbonitrile **29** (1.6 g, 4.54 mmol) , (*S*)-2-(4-hydroxy-phenylcarbamoyl)-pyrrolidine-1-carboxylic acid tert-butyl ester (2.78 g, 9.08 mmol) , copper iodide (865 mg, 4.54 mmol) , cesium carbonate (2.96 g, 9.08 mmol) and *N*,*N*-dimethyl glycine HCl salt (634 mg, 4.54 mmol) were divided into equal portions and loaded into 8 x 5 mL microwave vials. To each vial was added DMF (1.5 mL), and 1,4-dioxane (1.5 mL) and then each vial was capped and sealed. Each reaction vessel was heated in a microwave reactor at 140°C for 40 minutes . The reaction mixtures were then combined and concentrated to give a brown residue. Ethyl acetate (100 mL) was added and the mixture filtered. The solids on the filter were washed with ethyl acetate (2 x 200 mL) before the combined. Organic filtrates were washed with water (2 x 200 mL), brine, dried (filtered though a phase separator paper) and then evaporated to give 3.3 g of crude product. The product was purified by flash silica

chromatography, elution gradient 10% to 50% ethyl acetate in cyclohexane to afford **30** (1.30 g, 50%) as a yellowish solid. LCMS (ES^+) 578 $(M+H)^+$. ^1H NMR δ ($CDCl_3$): 7.57 (t, *J* = 9.2 Hz, 2H), 7.24 (dd, *J* = 9.2, 2.2 Hz, 1H), 7.02 (m, 4H), 5.76 (s, 2H), 4.50 (br s, 1H), 3.56 (t, *J* = 8.3 Hz, 2H), 4.50 (m, 1H), 3.49 – 3.30 (m, 2H), 2.58 (m, 1H), 2.03 – 1.88 (m, 3H), 1.59 (m, 1H), 1.52 (s, 9H), 1.43 (m, 1H), -0.05 (s, 9H).

***tert*-Butyl (2*S*)-2-[[4-[(3-cyano-1*H*-indazol-5-yl)oxy]phenyl]carbamoyl]pyrrolidine-1-carboxylate (31).** To *tert*-butyl (2*S*)-2-[[4-[3-cyano-1-(2-trimethylsilylethoxymethyl)indazol-5-yl]oxyphenyl]carbamoyl]pyrrolidine-1-carboxylate **30** (1.3 g, 2.25 mmol) was added tetrabutylammonium fluoride (1M in THF) (20 mL, 20 mmol) and the solution was stirred at 40°C for 18 hours. The solution was evaporated, water (150 mL) was added, and the mixture was extracted with ethyl acetate (2 x 150 mL). The combined organic layers were washed with brine, dried (filtered though a phase separator paper) and evaporated to yield **31** (935 mg, 93%) as a yellow solid. LCMS (ES+) 448 $(M+H)^+$. ^1H NMR δ ($CDCl_3$) 9.53 (br s, 1H), 7.56 (m, 1H), 7.50 (d, *J* = 8.7 Hz, 2H), 7.21 (br s, 1H), 7.16 (d, *J* = 8.3 Hz, 1H), 6.92 (m, 2H), 4.53 (m, 1H), 3.58 – 3.28 (m, 3H), 2.45 (m, 1H), 1.95 (m, 2H), 1.67 (m, 1H), 1.50 (s, 9H).

(2*S*)-*N*-[4-[3-Cyano-1-[(3,5-dimethylisoxazol-4-yl)methyl]indazol-5-yl]oxyphenyl]pyrrolidine-2-carboxamide (33). To *tert*-butyl (2*S*)-2-[[4-[(3-cyano-1*H*-indazol-5-yl)oxy]phenyl]carbamoyl]pyrrolidine-1-carboxylate **31** (118 mg, 0.26 mmol) in THF (4.5 mL) at -5°C under nitrogen was added 4-(chloromethyl)-3,5-dimethyl-isoxazole (0.04 mL, 0.25 mmol). The mixture was stirred at 0°C for 15 minutes then NaH (60% in mineral oil) (11 mg , 0.28 mmol) was added in one portion. The mixture was then stirred for another 30 minutes at 0°C, warmed to room temperature and stirred for 2 hours, then stirred at 40°C for a further 2 hours. Water (1 mL) was added, then the organic solvent was removed by evaporation. Ethyl

acetate (50 mL) was added and the mixture was washed with brine (50 mL), dried (filtered though a phase separator paper) and evaporated to give 300 mg of crude product. The product was purified by purified flash silica chromatography, elution gradient 20% to 60% ethyl acetate in cyclohexane to afford **32** (78 mg, 54%) as a glassy solid. The intermediate was dissolved in DCM (2 mL) and to this solution was added trifluoroacetic acid (0.8 mL). The solution was stirred at room temperature for 1 hour and the solvents were evaporated before the crude product was purified by flash silica chromatography, elution gradient 0% to 10% methanol in DCM to afford impure product which was further purified by prep LCMS (method D) to give **33** (18 mg, 15%) as a white solid. HRMS ESI+ *m/z* observed 457.19821, $C_{25}H_{25}N_6O_3$ requires 457.19827. ^{1}H NMR δ (d^6-DMSO) 10.00 (s, 1H), 8.04 (d, *J* = 9.1 Hz, 1H), 7.71 (d, *J* = 9.0 Hz, 2H), 7.40 (dd, *J* = 9.1, 2.0 Hz, 1H), 7.21 (d, *J* = 2.0 Hz, 1H), 7.05 (d, *J* = 9.0 Hz, 2H), 5.64 (s, 2H), 3.68 (dd, *J* = 8.8, 5.6 Hz, 1H), 3.31 (s, 1H), 2.88 (t, *J* = 7.6 Hz, 2H), 2.47 (s, 3H), 2.11 (s, 3H), 2.07 – 1.99 (m, 1H), 1.82 – 1.74 (m, 1H), 1.65 (m, 2H).

5-(4-Nitrophenoxy)-1*H*-indole (35). 1*H*-Indol-5-ol (**34**) (10 g, 75.1 mmol), 1-fluoro-4-nitro-benzene (10.6 g, 75.1 mmol) and cesium carbonate (29.36 g, 90.12 mmol) were stirred in DMF (100 mL) at room temperature for 16 hours. The mixture was partitioned between ethyl acetate (500 mL) and water (500 mL) and the organic layer was washed with water (3 x 300 mL) then brine (100 mL). The organic layer was dried ($MgSO_4$) and evaporated to yield crude product which was triturated with diethyl ether to afford 5-(4-nitrophenoxy)-1*H*-indole (**35**) (12.4 g, 65%) as a light brown solid. LCMS (ES^+) 254.94 $(M+H)^+$. ^{1}H NMR δ (d^6-DMSO) 11.30 (s, 1H), 8.21 (d, *J* = 9.3Hz, 2H), 7.50 (d, *J* = 8.6Hz, 1H), 7.45 (t, *J* = 2.8Hz, 1H), 7.36 (d, *J* = 2.3Hz, 1H), 7.05 (d, *J* = 9.3Hz, 2H), 6.91 (dd, *J* = 8.6, 2.3Hz, 1H), 6.46 (m, 1H).

4-(1*H*-indol-5-yloxy)aniline (36). 5-(4-Nitrophenoxy)-1*H*-indole **35** (2.0 g, 7.87 mmol) was dissolved in methanol (40 mL) and to the mixture was added to 10% palladium on charcoal (0.2 g) under nitrogen. The reaction vessel was evacuated and flushed with nitrogen (x 3) then evacuated and flushed with hydrogen (x 3). The reaction mixture was stirred under an atmosphere of hydrogen for 3 hours before being flushed with nitrogen and filtered through celite and washed with methanol. The filtrate was evaporated to afford 4-(1*H*-indol-5-yloxy)aniline (**36**) (1.77 g, 100%) as a light brown solid. LCMS (ES+) 224.99 $(M+H)^+$. ^{1}H NMR δ (d^6-DMSO) 11.03 (br s, 1H), 7.35 – 7.28 (m, 2H), 6.98 (d, *J* = 2.3Hz, 1H), 6.76 (dd, *J* = 8.7Hz, 2.3Hz, 1H), 6.71 (d, *J* = 8.8Hz, 2H), 6.55 (d, 8.8Hz, 2H), 6.32 (m, 1H), 4.85 (br s, 2H).

***tert*-Butyl (2*S*)-2-[[4-(1*H*-indol-5-yloxy)phenyl]carbamoyl]pyrrolidine-1-carboxylate (37).** 4-(1*H*-indol-5-yloxy)aniline **36** (1.77 g, 7.89 mmol), (2*S*)-1-*tert*-butoxycarbonylpyrrolidine-2-carboxylic acid (2.21 g, 10.26 mmol), *N,N,N′,N′*-tetramethyl-*O*-(1*H*-benzotriazol-1-yl)uronium hexafluorophosphate (4.49 g, 11.84 mmol) and diisopropylethylamine (2.04 g, 15.79 mmol) were stirred in DCM (50 mL) for 3 hours. The reaction mixture was partitioned between DCM (200 mL) and water (200 mL) then the organic layer was dried ($MgSO_4$) and evaporated to afford a brown oil. The crude product was purified by flash silica chromatography, elution gradient 0% to 40% ethyl acetate in cyclohexane to afford **37** (3.2 g, 96%) as an oily foam. LCMS (ES^+) 422.34 $(M+H)^+$. ^{1}H NMR δ (d^6-DMSO) 11.13 (br s, 1H), 9.92 (d, *J* = 6.7Hz, 1H), 7.57 – 7.51 (m, 2H), 7.42 – 7.35 (m, 2H), 7.17 – 7.12 (m, 1H), 6.88 (d, *J* = 8.9Hz, 2H), 6.84 – 6.76 (m, 1H), 6.37 (m, 1H), 4.28 – 4.15 (m, 1H), 3.42 (m, 1H), 2.24 – 2.10 (m, 1H), 1.94 – 1.75 (m, 3H), 1.40 (s, 4H), 1.29 (s, 5H). Amide NH not observed.

***tert*-Butyl (2*S*)-2-[[4-[(3-bromo-1*H*-indol-5-yl)oxy]phenyl]carbamoyl]pyrrolidine-1-carboxylate (38).** *tert*-Butyl (2*S*)-2-[[4-(1*H*-indol-5-yloxy)phenyl]carbamoyl]pyrrolidine-1-

carboxylate **37** (3.2 g, 7.59 mmol) was dissolved in DMF (50 mL) under nitrogen and *N*-bromosuccinimide (1.35 g, 7.59 mmol) was added portionwise. The reaction mixture was stirred at room temperature for 3 hours before being partitioned between water (400 mL) and ethyl acetate (400 mL). The organic layer was washed with water (3 x 300 mL) then dried ($MgSO_4$) and evaporated to afford a brown foam. The crude product was purified by flash silica chromatography, elution gradient 10% to 50% ethyl acetate in cyclohexane to afford **38** (3.3 g, 87%) as a clear oil. LCMS (ES^+) 500.31, 502.25 $(M+H)^+$. ^1H NMR δ (d^6-DMSO) 11.52 (br s, 1H), 9.96 (d, J = 5.92, 1H), 7.61 – 7.55 (m, 3H), 7.48 – 7.43 (m, 1H), 6.97 – 6.88 (m, 4H), 4.28 – 4.13 (m, 1H), 3.46 – 3.35 (m, 1H), 2.24 – 2.10 (m, 1H), 1.94 – 1.75 (m, 3H), 1.40 (s, 4H), 1.29 (s, 5H). Amide NH not observed.

(2*S*)-*N*-[4-[[3-(1-Methylpyrazol-4-yl)-1*H*-indol-5-yl]oxy]phenyl]pyrrolidine-2-carboxamide (40). *tert*-Butyl (2*S*)-2-[[4-[(3-bromo-1*H*-indol-5-yl)oxy]phenyl]carbamoyl]pyrrolidine-1-carboxylate **38** (0.05 g, 0.10 mmol), 1-methyl-4-(4,4,5,5-tetramethyl-1,3,2-dioxaborolan-2-yl)pyrazole (0.04 g, 0.20 mmol) and palladium tetrakistriphenylphosphine (6 mg, 0.005 mmol) were stirred in 1,4-Dioxane (0.75 mL). 1M K_3PO_4 solution in water (0.2 mL, 0.2 mmol) was added and the mixture was degassed and placed under a nitrogen atmosphere. The reaction mixture was heated to 150°C for 10 minutes in the microwave reactor and then partitioned between ethyl acetate (20 mL) and water (20 mL). The organic layer was dried ($MgSO_4$) and evaporated. The residue was dissolved in DCM (1 mL), TFA (1 mL) was added and then stirred for 30 minutes at room temperature. The mixture was evaporated then purified by prep LCMS (Method B), fractions containing product were then free based by absorbing onto a 1 g SCX cartridge, washing with methanol then eluting with 2M ammonia in methanol. Fractions containing the desired product were evaporated under a stream of nitrogen then in a vacuum

oven at 40°C to afford **40** (12 mg, 30%) as a white solid. HRMS ESI+ *m/z* observed 402.19244, $C_{23}H_{24}N_5O_2$ requires 402.19245. ^{1}H NMR δ (d^6-DMSO) 11.19 (br s, 1H), 9.90 (br s, 1H), 8.04 (s, 1H), 7.70 (s, 1H), 7.62 – 7.55 (m, 3H), 7.44 – 4.40 (m, 2H), 6.88 – 6.82 (m, 3H), 3.85 (s, 3H), 3.69 (m, 1H), 3.00 (br s, 1H), 2.89 (, *J* = 6.6Hz t, 2H), 2.10 – 1.98 (m, 1H), 1.81 - 1.73 (m, 1H), 1.68 – 1.61 (m, 2H).

***tert*-Butyl (2*S*)-2-[[4-(3-bromo-1-methyl-indol-5-yl)oxyphenyl]carbamoyl]pyrrolidine-1-carboxylate (41).** *tert*-Butyl (2*S*)-2-[[4-[(3-bromo-1*H*-indol-5-yl)oxy]phenyl]carbamoyl]pyrrolidine-1-carboxylate **38** (0.1 g, 0.20 mmol) was dissolved in DMF (2 mL) and cesium carbonate (0.098 g, 0.30 mmol) was added followed by iodomethane (0.034 g, 0.24 mmol). The reaction mixture was stirred at room temperature for 3 hours before being partitioned between ethyl acetate (20 mL) and water (20 mL). The organic layer was washed with water (2 x 20 mL) then dried ($MgSO_4$) and evaporated to afford **41** (0.09 g, 88%) as a light brown solid. LCMS (ES$^+$) 513.98, 515.94 (M+H)$^+$. ^{1}H NMR δ (d^6-DMSO) 9.95 (br s, 1H), 7.61 – 7.52 (m, 4H), 7.02 – 6.88 (m, 4H), 4.27 – 4.14 (m, 1H), 3.81 (s, 3H), 3.4 (m, 1H), 2.25 – 2.12 (m, 1H), 1.95 – 1.75 (m, 3H), 1.40 (s, 4H), 1.29 (s, 5H). Amide NH not observed.

(2*S*)-*N*-[4-[1-Methyl-3-(1-methylpyrazol-4-yl)indol-5-yl]oxyphenyl]pyrrolidine-2-carboxamide (43). *tert*-Butyl (2*S*)-2-[[4-(3-bromo-1-methyl-indol-5-yl)oxyphenyl]carbamoyl]pyrrolidine-1-carboxylate **41** (0.09 g, 0.18 mmol), palladium tetrakistriphenylphosphine (10 mg, 0.09 mmol), 1-methyl-4-(4,4,5,5-tetramethyl-1,3,2-dioxaborolan-2-yl)pyrazole (73 mg, 0.35 mmol) and 1M K_3PO_4 solution (0.35 mL, 0.35 mmol) were stirred in 1,4-dioxane (1.5 mL). The reaction mixture was degassed and placed under a nitrogen atmosphere before being heated to 80°C for 16 hours. The mixture was then partitioned between ethyl acetate (10 mL) and water (10 mL). The organic layer was dried ($MgSO_4$) and

evaporated then purified by flash silica chromatography, elution gradient 50% to 100% ethyl acetate in cyclohexane to afford **42** as a yellow oil. The residue was dissolved in DCM (1 mL), treated with TFA (1 mL) and stirred for 10 minutes. The solution was evaporated then purified by prep LCMS (Method A) then free based by absorbing onto a 1 g SCX cartridge, washing with methanol then eluting with 2M ammonia in methanol. Fractions containing desired product were evaporated under a stream of nitrogen then in a vacuum oven at 40°C to afford **43** (0.02 g, 26%) as a white glassy solid. HRMS ESI+ *m/z* observed 416.2072, $C_{24}H_{25}N_5O_2$ requires 416.2087. ^{1}H NMR δ (d^6-DMSO) 9.88 (s, 1H), 8.04 (s, 1H), 7.67 (s, 1H), 7.62 – 7.57 (m, 3H), 7.49 (d, *J* = 8.8Hz, 1H), 7.43 (d, *J* = 2.2Hz, 1H), 6.91 (dd, *J* = 8.8Hz, 2.2Hz, 1H), 6.86 (d, *J* = 9.0Hz, 2H), 3.85 (s, 3H), 3.81 (s, 3H), 3.67 (m, 1H), 3.05 – 2.95 (br s, 1H), 2.88 (t, *J* = 6.6Hz, 2H), 2.07 – 1.97 (m, 1H), 1.80 – 1.70 (m, 1H), 1.67 – 1.60 (m, 2H).

Associated Content

Supporting Information Available Protocols are provided for the enzyme and cell assays, synthetic methods for the remaining examples, together with crystallographic information, and kinase panel selectivity data for compound **26**. This material is available free of charge via the Internet at http://pubs.acs.org.

Corresponding Author Information Jason G. Kettle Tel: +441625517920, jason.kettle@astrazeneca.com

References

(1) Warburg, O. On respiratory impairment in cancer cells. *Science* **1956**, *124*, 269-270.

(2) Castell, F.; Cook, G. J. Quantitative techniques in 18FDG PET scanning in oncology. *Br. J. Cancer* **2008**, *98,* 1597-1601.

(3) Mansour, T. E. Studies on heart phosphofructokinase: purification, inhibition and activation. *J. Biol. Chem.* **1963**, *238*, 2285-2292.

(4) Van Schaftingen, E.; Hue, L.; Hers, H. G. Fructose 2,6-bisphosphate, the probable structure of the glucose- and glucagon-sensitive stimulator of phosphofructokinase. *Biochem. J.* **1980**, *192*, 897-901.

(5) Pilkis, S. J.; Claus, T. H.; Kurland, I. J.; Lange, A. J. 6-Phosphofructo-2-kinase/fructose-2,6-bisphosphatase: a metabolic signalling enzyme. *Annu. Rev. Biochem.* 1995, *64*, 799-835.

(6) Okar, D. A.; Manzano, A.; Navarro-Sabate, A.; Riera, L.; Bartrons, R.; and Lange, A. J. PFK2/FBPase-2: maker and breaker of the essential biofactor fructose-2,6-bisphosphate. *Trends Biochem. Sci.* **2001**, *26*, 30-35.

(7) Sakakibara, R.; Kato, M.; Okamura, N.; Nakagawa, T.; Komada, Y.; Tominaga, N.; Shimojo, M.; Fukasawa, M. Characterization of a Human Placental Fructose-6-Phosphate-2-Kinase/Fructose-2,6-Bisphosphatase. *Biochem. J.* **1997**, *122*, 122-128.

(8) Atsumi, T.; Chesney, J.; Metz, C.; Leng, L.; Donnelly, S.; Makita, Z.; Mitchell, R.; Bucala, R. High expression of inducible 6-phosphofructo-2-kinase/fructose-2,6-bisphosphatase (iPFK2; PFKFB3) in human cancers. *Cancer Res.* **2002**, *62*, 5881-5887.

(9) Bando, H.; Atsumi, T.; Nishio, T.; Niwa, H.; Mishima, S.; Shimizu, C.; Yoshioka, N.; Bucala, R.; Koike, T. Phosphorylation of the 6-phosphofructo-2-kinase/fructose 2,6-bisphosphatase/PFKFB3 family of glycolytic regulators in human cancer. *Clin. Cancer Res.* **2005**, *11*, 5784-5792.

(10) Telang, S.; Yalcin, A.; Clem, A. L.; Bucala, R.; Lane, A. N.; Eaton, J. W.; Chesney, J. Ras transformation requires metabolic control by 6-phosphofructo-2-kinase. *Oncogene* **2006**, *25*, 7225-7234.

(11) Minchenko, O.; Opentanova, I.; Caro, J. Hypoxic regulation of the 6-phosphofructo-2-kinase/fructose-2,6-bisphosphatase gene family (PFKFB-1-4) expression in vivo. *FEBS Lett.* **2003**, *554*, 264-270.

(12) Obach, M.; Navarro-Sabate, A.; Caro, J.; Kong, X.; Duran, J.; Gomez, M.; Perales, J.C.; Ventura, F.; Rosa, J.L.; Bartrons, R. 6-Phosphofructo-2-kinase (pfkfb3) gene promoter contains hypoxia-inducible factor-1 binding sites necessary for transactivation in response to hypoxia. *J. Biol. Chem.* **2004**, 279, 53562-53570.

(13) Colombo, S. L.; Palacios-Callender, M.; Frakich, N.; De Leon, J.; Schmitt, C. A.; Boorn, L.; Davis, N.; Moncada, S. Anaphase-promoting complex/cyclosome-Cdh1 coordinates glycolysis and glutaminolysis with transition to S phase in human T lymphocytes. *Proc. Natl. Acad. Sci. U. S. A.* **2010**, *107*, 18868-18873.

(14) Herrero-Mendez, A.; Almeida, A.; Fernandez, E.; Maestre, C.; Moncada, S.; and Bolanos, J. P. The bioenergetic and antioxidant status of neurons is controlled by continuous degradation of a key glycolytic enzyme by APC/C-Cdh1. *Nat. Cell Biol.* **2009**, *11*, 747-752.

(15) Clem, B.; Telang, S.; Clem, A.; Yalcin, A.; Meier, J.; Simmons, A.; Rasku, M. A.; Arumugam, S.; Dean, W. L.; Eaton, J.; Lane, A.; Trent, J. O.; Chesney, J. Small-molecule inhibition of 6-phosphofructo-2-kinase activity suppresses glycolytic flux and tumor growth. *Mol. Cancer Ther.* **2008**, *7*, 110-120.

(16) Clem, B. F.; O'Neal, J.; Tapolsky, G.; Clem, A. L.; Imbert-Fernandez, Y.; Kerr, D. A.; Klarer, A. C.; Redman, R.; Miller, D. M.; Trent, J. O.; Telang, S.; Chesney, J. Targeting 6-

phosphofructo-2-kinase (PFKFB3) as a therapeutic strategy against cancer. *Mol. Cancer Ther.* **2013**, *12*, 1461-1470.

(17) Brooke, D. G.; van Dam, E. M.; Watts, C. K. W.; Khoury, A.; Dziadek, M.A.; Brooks, H.; Graham, L.J.K.; Flanagan, J.U.; Denny, W.A. Targeting the Warburg Effect in cancer; relationships for 2-arylpyridazinones as inhibitors of the key glycolytic enzyme 6-phosphofructo-2-kinase/2,6-bisphosphatase 3 (PFKFB3). *Bioorg. Med. Chem.* **2014**, *22,* 1029-1039**.**

Table of Contents Graphic